General Disclaimer

One or more of the Following Statements may affect this Document

- This document has been reproduced from the best copy furnished by the organizational source. It is being released in the interest of making available as much information as possible.

- This document may contain data, which exceeds the sheet parameters. It was furnished in this condition by the organizational source and is the best copy available.

- This document may contain tone-on-tone or color graphs, charts and/or pictures, which have been reproduced in black and white.

- This document is paginated as submitted by the original source.

- Portions of this document are not fully legible due to the historical nature of some of the material. However, it is the best reproduction available from the original submission.

NASA TM X- 70920

PHOTONUCLEAR INTERACTIONS OF ULTRAHIGH ENERGY COSMIC RAYS AND THEIR ASTROPHYSICAL CONSEQUENCES

J. L. PUGET
F. W. STECKER
J. H. BREDEKAMP

JULY 1975

GSFC ——— GODDARD SPACE FLIGHT CENTER ———
GREENBELT, MARYLAND

PHOTONUCLEAR INTERACTIONS OF ULTRAHIGH ENERGY

COSMIC RAYS AND THEIR ASTROPHYSICAL CONSEQUENCES

J. L. Puget*

F. W. Stecker

J. H. Bredekamp

Theoretical Studies Group

NASA Goddard Space Flight Center

Greenbelt Maryland 20771

*NAS/NRC Postdoctoral Resident Research Associate; Permanent Address:

Observatoire de Meudon, Meudon, France

2

ABSTRACT:

We present here the results of detailed Monte Carlo calculations of the interaction histories of ultrahigh energy cosmic-ray nuclei with intergalactic radiation fields using improved estimates of these fields and empirical determinations of photonuclear cross sections including multinuclear disintegrations for nuclei up to ^{56}Fe. Intergalactic and galactic energy loss rates and nucleon loss rates for nuclei up to ^{56}Fe are also given. Astrophysical implications are discussed in terms of expected features in the cosmic-ray spectrum between 10^{18} and 10^{21} eV for the universal and supercluster origin hypotheses. The results of these calculations indicate that ultrahigh energy cosmic rays cannot be universal in origin regardless of whether they are protons or nuclei. Both the supercluster and galactic origin hypotheses, however, are possible regardless of nuclear composition.

1. Introduction.

The basic interactions between photons and nuclei of ultrahigh energy which have important astrophysical consequences are:

1) Compton interactions,

2) Pair production (particulary of e^+e^- pairs) in the field of the nucleus,

3) Photodisintegration of the nucleus,

4) photoproduction of hadrons

In the rest-system of the nucleus, process (1) has no threshhold energy, process (2) occurs at a threshhold energy of $2m_ec^2 \simeq 1$ MeV, process (3) is particularly important in most cases between 15 and 25 MeV where the giant dipole resonance has its peak, and process (4) has a threshhold energy of

$$\varepsilon'_{th} = m_\pi c^2(1+m_\pi/2m_p) \simeq 145 \text{ MeV} \qquad (1)$$

Process (1), Compton effect interactions involving nuclei, is a process which results in only a negligibly small energy loss for the nuclei given by

$$-\frac{dE}{dt} = \frac{4}{3}\rho_\gamma\sigma_Tc\left(\frac{m_e}{Am_p}\right)^2 Z^4 \left(\frac{E}{Am_pc^2}\right)^2 = \frac{Z^4}{A^4}\rho_\gamma\left(\frac{E}{Am_pc^2}\right)^2\frac{\text{eV}}{\text{s}} \quad (2)$$

where ρ_γ is the energy density of the ambient photon field in eV cm^{-3}, σ_T is the Thomson cross section and Z and A are the atomic number and weight of the nucleus with E being the total energy of the nucleus in eV.

Processes (2) through (4) must be considered in investigating the propagation ultrahigh energy cosmic ray nuclei in intergalactic space (Greisen 1966, Zatsepin and Kuz'min 1966, Stecker 1968,1969, Berezinskii and Zatsepin 1971).

Process (2), particularly important for heavy nuclei, has been treated in detail in its astrophysical context by Blumenthal (1970). This process is only of importance for interactions with the 2.7 K blackbody background radiation (see section 4). In this case, for interactions with a blackbody field of temperature T, the photon density is given by the Planck function

$$n(\varepsilon) = (\hbar c)^{-3} (\varepsilon/\pi)^2 (e^{\varepsilon/kT} - 1)^{-1} \tag{3}$$

and the energy loss rate for the nucleus is

$$-(dE/dt) = 3\alpha\sigma_T h^{-3} Z^2 (m_e c^2 kT)^2 f\{m_e c^2/(2\gamma kT)\} \tag{4}$$

where $f(\nu)$ is shown in Figure 1. The Lorentz factor of the nucleus $\gamma = E(Am_p c^2)^{-1}$.

The photohadron production process (4) is dominated by photopion production channels. This process has been treated in detail in a previous paper (Stecker 1968). Figure 2 shows the lifetime and mean free path for protons against attenuation by energy loss due to pair production (Blumenthal 1970) and photomeson production (Stecker 1968), due to interactions with the 2.7 K radiation. Also shown in Figure 2 is the lifetime for ^{56}Fe against energy loss by e^+e^- pair production.

Process (3), photodisintegration, is not as easy to treat as the other processes and most previous cosmic ray papers have used only simple estimates of the cross section for this process. Stecker (1969) used a detailed study of ^4He photodisintegration (Gorbunov 1968) to determine the lifetime of ^4He and estimate

the lifetime of ^{56}Fe against one nucleon loss by interactions with the 2.7 K radiation. The main emphasis in this paper will be on a presentation of the results of a new and much more detailed calculation of the intergalactic photodisintegration of ultrahigh energy nuclei with the following improvements:

1) Use of empirically determined cross section data as a function of energy for all nuclei with $1 \leq A \leq 56$. It is exactly in this mass range where contributions from nonresonant photonuclear disintegration processes are most significant. Because of the position of ^{56}Fe on the binding energy curve, it is considered to be a significant end product of stellar evolution and higher mass nuclei are found to be much rarer in the cosmic radiation.

2) Use of cross section data for $1 \leq A \leq 56$ for <u>multinucleon emission</u> interactions as well as single nucleon emission interactions. Multinucleon losses (except for double nucleon loss) involve non-resonant processes and are particularly important at energies between the position of the giant dipole resonance and the pion production threshhold (i.e., 25 MeV$< \epsilon' <$145 MeV , see section 2).

3) Use of new estimates of the intergalactic infrared radiation field, whose effect is included along with that of the blackbody radiation.

4) Inclusion of energy loss by pair production occuring concurrently with energy loss by photodisintegration.

5) Treatment of these concurrent energy loss processes by using numerical Monte Carlo techniques which also allow a natural treatment of the multinucleon loss processes in a determination of the photodisintegration and energy loss

histories of nuclei as a function of initial energy.

2. The Photodisintegration Process.

A general discussion of the photonuclear interaction process for the energies of interest here has been given by Danos and Fuller (1965) and Hayward (1970). This energy band, extending up to 150 MeV, or about the meson production threshold, rather naturally splits into two parts. The lower region, extending up to 30 MeV, has been studied extensively. This is the domain of the giant resonances of the nuclear photoeffect. Here, although two-nucleon emission does take place, most of the absorption cross section results in the emission of only single nucleons, either neutrons or protons. For the medium and heavy nuclei, $A \geq 50$, the total photon absorption cross section can be well represented by a single, or in the case of the deformed nuclei, by the superposition of two Lorentzian curves of the form

$$\sigma(\varepsilon') = \sigma_0 \frac{\varepsilon'^2 \, \Gamma_d^2}{(\varepsilon_0'^2 - \varepsilon'^2)^2 + \varepsilon'^2 \Gamma_d^2} \tag{5}$$

For the lighter nuclei, the absorption cross section often shows considerably more structure than this. For all nuclei the basic photonuclear interaction at these energies is pictured as being with the individual uncorrelated nucleons comprising the nucleus. In the shell model language, the interaction results in the creation of particle-hole pairs. The collective giant resonance state is described by a coherent superposition of individual single-particle transitions.

The data for energies between 30 and 150 MeV are relatively sparse. The available measurements seem to indicate that the total cross section in this region is a relatively smooth function of energy. Reactions in which a number of nucleons are emitted seem to make up most of the total absorption cross section.

In this region the photon's wavelength becomes comparable to, and less than, nuclear dimensions and it becomes very difficult to conserve both energy and momentum in a single-particle interaction within the nucleus. The dominant absorption process is then pictured as one in which the photon interacts with a nucleon pair while they are scattering within the nucleus. This is referred to as the quasi-deuteron effect. (Levinger, 1951).

In the following discussion, the strength of a photonuclear reaction in the two energy regions, i.e., the integral of the cross section over the energy interval, will be given in units of the classical dipole sum rule, i.e.,

$$\Sigma_d = \int \sigma(\varepsilon') \, d\varepsilon' = \frac{2\pi^2 e^2}{Mc} \, \frac{NZ}{A} = 59.8 \, \frac{NZ}{A} \quad \text{MeV-mb} \tag{6}$$

where M is the nucleon mass, A the mass number, Z the number of protons, and N the number of neutrons in the nucleus. The derivation of this result is based on both the long wavelength approximation for the dipole operator involving nucleon coordinates only and on closure, i.e., it assumes that the integration in Eq. (6) is carried out over all excitation energies. Meson coordinates within nuclei are specifically ignored. Since these assumptions are not valid for the excitations being considered here, no real physical significance should be attached to this normalization. It is simply a convenient scale factor that removes the principal dependence of the total absorption cross section on N, Z, and A.

The data used in these calculations were based on an evaluation of the information in the files of the Photonuclear Data Center at the National Bureau of Standards (E. G. Fuller, private communication). To simplify these calculations, the observed detailed dependence of the various reaction cross sections on photon energy was not used. Rather, each cross section was assumed to be independent of energy over a finite energy band of width Δ. For energies below 30 MeV, this band is assumed to be centered about a mean energy ε_0' for each reaction. As a further simplification, it was assumed that the half-lives of the various reaction

products resulting from photonuclear reactions were all short compared to the rate at which the reactions take place. With this assumption, it was not necessary to consider each individual reaction but rather only the cross section for emitting ΔA nucleons from a nucleus of mass A had to be input into the calculations.

The data used in the calculations are given in Tables 1 and 2. For energies below 30 MeV, the total absorption cross section is assumed to result in reactions in which only one or two nucleons are emitted. These are given in terms of the quantities ε_o', ξ, and Δ listed in Table 1 with the subscripts 1 or 2, respectively. For each reaction, these were defined as follows:

$$\xi_1 = \frac{1}{\Sigma_d} \int_0^{30} \sigma^{(1)}(\varepsilon')d\varepsilon' \qquad (7)$$

where $\sigma^{(1)}(\varepsilon')$ is the actual single nucleon emission cross section as a function of photon energy ε'.

$\varepsilon_{o,1}'$ the mean energy for the reaction $\sigma^{(1)}(\varepsilon')$ chosen by inspection of a graph of the cross section as a function of ε'.

$$\Delta_1 \sigma_m = \int_0^{30} \sigma^{(1)}(\varepsilon')d\varepsilon' \qquad (8)$$

Δ_1 and σ_m were chosen so as to closely as possible match the actual dependence of $\sigma^{(1)}(\varepsilon')$ on energy.

The corresponding quantities for the two nucleon reactions were chosen in a similar way. As has been indicated previously, there are ample experimental data available for photon energies below 30 MeV to use in determining these parameters. For these excitation energies, the principal undertainties in the final results are probably those associated with the very crude parameterization used to describe the one and two nucleon emission cross sections as a function of energy.

The data for the region from 30 to 150 MeV are parameterized by two quantities, the total strength of the interaction given by ζ in Table 1, and a branching ratio given in Table 2. The total strength is given by:

$$\zeta = \frac{1}{\Sigma_d} \int_{30}^{150} \sigma_t(\varepsilon')d\varepsilon'$$

(9)

where $\sigma_t(\varepsilon')$ is the total photonuclear absorption cross section. The strength between 30 and 150 MeV was actually obtained by taking the difference between the estimated total strength to 150 MeV and a value for the measured strength in the region 0 to 30 MeV. The estimated total strength to 150 MeV as a function of Z was based to a large extent on an interpolation and extrapolation of the total cross section measurements made at Mainz (J. Ahrens et al., private communication, to be published in Nuclear Physics). These values are estimated to have an overall uncertainty of ±15%. The branching ratio data given in Table 2 for the nuclei heavier than Na are based on spallation product yields induced by bremsstrahlung with peak energies ranging from 150 to 240 MeV while the data for the lighter nuclei are based on the analysis of 170 MeV bremsstrahlung yields obtained from cloud chamber measurements. These data should not be taken to represent anything more than a first approximation of the yields that might be expected from a $1/\varepsilon'$ photon energy spectrum.

For the lighter elements it is found that only about half of a "dipole sum" as given by equation (6) is in the giant resonance and even for ^{39}K

only about 3/4 of the value given (6) is in the giant resonance. In the particular cases of elements with $A \lesssim 4$, the giant resonance does not play a role in the photodisintegration process (see later discussion).

One may also note that in terms of total integrated cross sections

$$\int_0^{30 \text{ MeV}} \sigma_t(\epsilon')d\epsilon' \quad \sim \quad \int_{30}^{150 \text{ MeV}} \sigma_t(\epsilon')d\epsilon' \tag{10}$$

which is another indication of the effect of nonresonant processes since higher order multipole resonances are considerably weaker than the dipole resonance.

Table 1. Cross Section Parameters for Photonuclear Emission Processes (ϵ and Δ in MeV)

A	$\epsilon'_{0,1}$	ξ_1	Δ_1	$\epsilon'_{0,2}$	ξ_2	Δ_2	ζ	Element
56	18	0.98	8	22	0.15	7	0.95	Fe
55	18	0.93	7	23.5	0.20	8	0.95	Mn
54	18	0.93	7	24	0.20	8	0.95	Cr
53	18	1.03	7	24	0.10	8	0.95	Cr
52	18	1.08	7	24	0.05	8	0.95	Cr
51	19	1.02	7	25	0.11	6	0.95	V
50	19	1.03	8	25	0.10	6	0.95	Ti
49	19	1.03	8	25	0.10	6	0.95	Ti
48	19	1.03	8	25	0.10	6	0.95	Ti
47	19	1.03	8	25	0.10	6	0.95	Ti
46	19	1.03	8	25	0.10	6	0.95	Ti
45	19	0.97	9	26	0.15	8	0.95	Sc
44	20	0.92	9	26	0.20	8	0.96	Ca
43	20	0.97	8	26	0.15	8	0.96	Ca
42	20	1.02	7	26	0.10	8	0.96	Ca
41	20	0.92	6	26	0.20	8	0.96	Ca
40	20	0.84	6	26	0.28	10	0.96	Ca
39	20	0.73	7	25	0.38	12	0.98	K
38	18	0.86	8	22	0.24	8	0.98	A
37	20	0.81	7	24	0.28	7	1.00	Cl
36	22	0.82	12	22	0.25	12	1.00	S
35	20	0.87	7	26	0.22	10	1.00	Cl
34	22	0.87	12	22	0.20	12	1.00	S
33	22	0.82	12	22	0.25	12	1.00	S
32	22	0.97	12	30	0.10	12	1.00	S
31	21	0.85	8	29	0.20	12	1.02	P
30	20	0.83	7	26	0.20	8	1.04	Si
29	20	0.83	7	26	0.20	8	1.04	Si
28	21	1.01	8	30	0.02	8	1.04	Si
27	21	0.80	8	29	0.20	12	1.05	Al
26	18	0.77	8	26	0.20	8	1.08	Mg
25	23	0.77	9	28	0.20	7	1.08	Mg
24	19	0.94	11	29	0.03	6	1.08	Mg
23	22	0.83	12	25	0.12	10	1.09	Na
22	22	0.81	12	21	0.11	4	1.09	Ne
21	22	0.84	12	25	0.08	6	1.09	Ne
20	22	0.87	12	26	0.05	8	1.09	Ne
19	23	0.76	14	29	0.14	14	1.10	F
18	24	0.67	9	29	0.20	10	1.10	O
17	24	0.77	9	29	0.20	10	1.10	O

Table 1, Continued

A	$\epsilon'_{0,1}$	ξ_1	Δ_1	$\epsilon'_{0,2}$	ξ_2	Δ_2	ζ	Element
16	24	0.83	9	30	0.04	10	1.10	O
15	23	0.73	10	23	0.10	10	1.07	N
14	23	0.46	10	23	0.37	10	1.07	N
13	23	0.71	8	27	0.05	8	1.06	C
12	23	0.76	6	- *	-	-	1.06	C
11	26	0.54	11	26	0.15	11	1.03	B
10	25	0.54	11	25	0.15	11	1.03	B
9	26	0.67	20	- *	-	-	1.00	B
4	27	0.47	12	45	0.11	40	1.11	He
3	13	0.33	18	15	0.33	13	1.11	He
2	5	0.97	-3,+15	-	-	-	-	H

*
Two nucleon emission negligible.

Table 2. Branching Ratios for i-nucleon Emission in the 30 MeV to
150 MeV Energy Range.

Nucleus	i	f_i	Main Channel
^{4}He	1	0.8	^{4}He (γ,n) ^{3}He, ^{4}He (γ,p) ^{3}H
	2	0.2	^{4}He (γ,np) ^{2}H
^{9}Be	1	1	^{9}Be (γ,n) 2 ^{4}He
^{10}B - ^{22}Ne	1	0.1	
	2	0.3	
	3	0.1	
	4	0.1	
	5	0.2	
	6	0.2	
^{23}Na - ^{56}Fe	1	0.10	
	2	0.35	
	3	0.10	
	4	0.05	
	5	0.15	
	6	0.045	
	7	0.04	
	8	0.035	
	9	0.03	
	10	0.025	
	11	0.02	
	12	0.018	
	13	0.015	
	14	0.012	
	15	0.01	

3. The Intergalactic Background Radiation Fields.

The background radiation of importance in determining the photonulear reaction rate in intergalactic space consists of the 2.7 K microwave radiation and the radiation fields of higher energy , viz., the infrared and the optical background radiation. The long wavelength radio background from extragalactic sources (Clark, et al. 1970) is of too low an energy and intensity to be of importance in the context of this paper.

a. The Microwave Radiation.

The 2.7 K radiation appears, for all practical purposes here, to be an ideal blackbody in the energy range 2×10^{-6} eV $< \varepsilon < 2 \times 10^{-3}$ eV (Peebles 1971, Thaddeus 1972, Hegyi et al. 1974, Robson et al, 1974, Woody et al. 1975). We assume it to be such in our calculations.

b. The Optical Radiation.

In considering the optical and infrared radiation in intergalactic space, one must keep in mind that even for measurements made outside the atmosphere, the measured background contains components from such nonextragalactic sources as Zodiacal light, emission from interplanetary and interstellar dust, and radiation from nearby stars at high galactic latitudes as well as halo stars. Because, therefore, only upper limits are available from direct measurements, the intergalactic infrared and optical radiation must be estimated using theoretical arguments.

Measurements of the fluctuations of the observed optical background on a small angular scale give upper limits on the contribution to the extra-galactic flux from discrete sources such as galaxies (Partridge 1974, Shectman 1974). The implied flux gives a value for the energy density of the optical radiation of $\sim 3 \times 10^{-3}$ eV cm^{-3} in the energy range 0.8 eV $< \varepsilon <$ 10 eV. This value precludes strong evolution of the luminosity function for galaxies (i.e., galaxies much brighter in the past) as has been discussed by Partridge and Peebles 1967a,b. Of course, a diffuse field of truly extragalactic origin (e.g., bremsstrahlung from a hot intergalactic gas) would not be detectable using fluctuation measurements, but we can assume that such radiation is relatively small (Field 1972).

We therefore assume an intergalactic dilute starlight field with a temp-erature of 5000 K and a dilution factor of 1.2×10^{-15} in our calculations. The effect of such a field is small, as previously noted in the case of a somewhat larger optical radiation field by Stecker (1969).

c. Infrared Radiation (2×10^{-3} eV to 0.8 eV).

Only experimental upper limits exist in the infrared energy range for the extragalactic background radiation (Pipher et al. 1971, Soifer et al. 1971, Houck et al. 1972, Meullner and Weiss 1972, Williamson et al 1973, McNutt and Feldman 1970, Hoffmann et al. 1973). Thus, we must rely on theoretical esti-mates of this radiation. Here, as in the case of the optical background rad-iation, we shall assume that the infrared background originates mainly in extragalactic objects. In the last four years it has been found that many of the active extragalactic objects such as quasars, N galaxies, the nuclei of Seyfert galaxies, and some radio galaxies as well, emit most of their energy

in the far infrared in the 30 to 100 μ range. Neugebauer et al (1971), Rieke and Low (1972) and Kleinman and Wright (1974) give fluxes at 10μ for 64 of these sources. For two sources, M82, and NGC 253, a continuous spctrum has been measured. Using these data, combined with the data of Schmidt (1971) on the luminosity function of extragalactic objects, it is possible to evaluate the contribution of these extragalactic objects to the infrared background. The data indicate that a typical extragalactic infrared source has a maximum in its spectrum between 30μ and 100μ and that the average spectral index of its energy spectrum on the high frequency side of the maximum is $\alpha \simeq 1.5$.

The effect of sources at high redshifts z can be estimated as follows: If one considers class of objects with a density evolution with redshift proportional to $(1 + z)^m$ (m = 3 being the case with no evolution and only geometrical expansion included)and we consider the part of their spectrum which has a power law form so that their intensity is given by

$$I(\nu) = I_0 \, \nu^{-\alpha} \quad \text{for} \quad \nu_m \leq \nu \leq \nu_M \tag{11}$$

their integrated contribution to the infrared background is then

$$F(\nu) = n_0 I_0 \nu^{-\alpha} (cH_0^{-1}/4\pi) \int_0^{z_M} dz \, (1+z)^{m-(\alpha+5)} (1+\Omega z)^{-1/2} \tag{12}$$

where H_0 is the Hubble constant and Ω is the fraction of the critical density.

The solution to equation (12) will give power law spectra in the frequency ranges $\nu_m (1+z_M)^{-1} \leq \nu \leq \nu_m$ and $\nu_m \leq \nu \leq \nu_M$ with a spectral index depending on the values of α and m.

If most quasars have a high infrared output compared with their output at other wavelengths, it then seems to be a likely possibility that there is a strong redshift evolution of their infrared luminosity as is found to be the case at optical wavelengths (m = 6). Considering the limited amount of observa-

tional data on Seyfert galaxies, both strong evolution (m=6) and no evolution (m=3) have been considered here in estimating their contribution to the infrared background. The fluxes from quasars and Seyfert galaxies, as well as the flux from normal galaxies with m=3, have been computed and the results of these calculations are shown in Figure 3.

Two power laws have been drawn on Figure 3 which can be considered as giving reasonable lower and upper limits on the intergalactic infrared flux. At very long wavelengths ($\sim$500μ) the major contribution to the infrared background is probably due to the diffuse component associated with the distortion of the 2.7 K blackbody spectrum due to effects associated with the early thermal history of the universe (Kompaneets 1957, Zel'dovich et al 1972, Chan and Jones 1975).

The power law spectra shown in Figure 3, which were employed in this paper , were taken to extend from the optical graybody radiation field to the microwave blackbody radiation field , will hereafter be designated as HIR (high infrared case) and LIR (low infrared case. They are given in terms of photon density spectra by the numerical expressions

$$\text{HIR:} \quad n(\varepsilon) = 1.1 \times 10^{-3} \, \varepsilon^{-2.5} \quad (cm^{-3}eV^{-1})$$

and   (13)

$$\text{LIR:} \quad n(\varepsilon) = 2.6 \times 10^{-3} \, \varepsilon^{-2} \quad (cm^{-3}eV^{-1})$$

with the photon energies given in eV and the spectra extending over the energy range between 2×10^{-3} eV and 0.8 eV.

4. Calculation of the Intergalactic Nucleon and Energy Loss Rates.

The photodisintegration rate for a nucleus of mass A with the sub-
sequent release of i nucleons is given by the expression

$$R_{A,i} = \frac{1}{2} \gamma_A^{-2} \int_0^\infty d\varepsilon \, \varepsilon^{-2} n(\varepsilon) \int_0^{2\gamma_A\varepsilon} d\varepsilon' \, \varepsilon' \, \sigma_{A,i}(\varepsilon') \qquad (14)$$

(Stecker 1969) where $n(\varepsilon)$ is the photon density of the ambient radiation
with energy ε in the observers system (see previous section), ε' is the
energy of the photon in the rest system of the cosmic ray nucleus and γ_A is the
Lorentz factor of the nucleus.

Because, as was discussed in section 2, there can exist large and
significant deviations from the pure Lorentzian shape in the energy range
where the maximum cross section occurs, a Gaussian approximation for the
cross section for 1 and 2 nucleon disintegrations in this energy range was
found to be useful both as an adequate fit to the cross section data and as
an expedient in performing the numerical calculations. This choice, in con-
juction with a threshhold energy of 2 MeV in the rest system of the nucleus
and a constant cross section above 30 MeV, was numerically found to give
rates which were very similar to those given by a Lorentian over the resonance
region where integrated over the photon density function used in equation (14)
as discussed in the previous section. The error introduced by this approximation
was found to be relatively small compared to the other uncertainties involved
in this calculation. Relatively more important, was the consideration of multi-
nucleon emission channels which, when weighted by the number is nucleons emitted,
can be seen to have an important effect of the total nucleon and energy loss
rates. This can be seen from an examination of the branching ratios for multi-

19

nucleon emission given in table 2.

The cross sections used for evaluating equation (14) were of the form

$$\sigma_{A,i} = W^{-1} \xi_{A,i} Z_d \Delta^{-1} \theta_+(2) \theta_-(30) \exp\left[-2\left(\frac{\epsilon'-\epsilon'_{0,i}}{\Delta_i}\right)^2\right] + \frac{5 f_i \Sigma_d \theta_+(30)}{120} \tag{15}$$

for i = 1, 2 , and

$$\sigma_{A,i} = \frac{5 f_i \Sigma_d \theta_+(30)}{120} \qquad\qquad \text{for } i > 2 \tag{16}$$

where all the energies are in MeV and the normalization factor

$$W = \left(\frac{\pi}{8}\right)^{1/2}\left[\text{Erf}\left(\frac{30-\epsilon'_{0,i}}{2^{-1/2}\Delta}\right) + \text{Erf}\left(\frac{\epsilon'_{0,i}-2}{2^{-1/2}\Delta}\right)\right] \tag{17}$$

with

$$\text{Erf}(x) = 2\pi^{-1/2}\int_0^x e^{-t^2} dt \tag{18}$$

and

$$\theta_+(x) = \begin{cases} 1 & \epsilon' \geqslant x \\ 0 & \epsilon' < x \end{cases} \tag{19}$$

$$\theta_-(x) = \begin{cases} 0 & \epsilon' > x \\ 1 & \epsilon' \leqslant x \end{cases}$$

By substituting equations (15) through (19) in equation (14), the photodisintegration rates can be expressed as sums of integrals of four

basic forms. The first is

$$I_1 = \frac{C_1}{2\gamma_A^2}\left[\int_{2/2\gamma}^{30/2\gamma} d\epsilon \, (e^{-\epsilon/kT} -1)^{-1} J(\epsilon) + \int_{30/2\gamma}^{\infty} d\epsilon \, (e^{-\epsilon/kT} -1)^{-1} J'(\epsilon) \right] \tag{20}$$

for integrations of the Gaussian part of the cross section over a thermal photon field where

$$C_1 = (\pi^2 \hbar^3 c^3)^{-1} D W^{-1} \xi_{A,i} \Sigma_d \Delta^{-1} \tag{21}$$

D being a dilution factor for the case of starlight optical radiation (graybody) which is equal to unity for pure blackbody radiation. The functions $J(\epsilon)$ and $J'(\epsilon)$ are given by the expressions

$$J(\epsilon) = \int_{2\,MeV}^{2\gamma\epsilon} x \, e^{-2\left(\frac{x-\epsilon_{0,i}'}{\Delta}\right)^2} dx = \left(\frac{\pi}{8}\right)^{1/2} \epsilon_{0,i}' \Delta \left[\text{sign}\,(2\gamma\epsilon - \epsilon_{0,i}')\, \text{Erf}\left(\frac{2\gamma\epsilon - \epsilon_{0,i}'}{2^{-1/2}\Delta}\right) \right.$$

$$\left. + \text{Erf}\left(\frac{\epsilon_{0,i}' - 2}{2^{-1/2}\Delta}\right) \right] + \left(\frac{\Delta}{2}\right)^2 \left\{ \exp\left[-2\left(\frac{\epsilon_{0,i}' - 2}{\Delta}\right)^2\right] \right. \tag{22}$$

$$\left. - \exp\left[-2\left(\frac{2\gamma\epsilon - \epsilon_{0,i}'}{\Delta}\right)^2\right] \right\}$$

and

$$J'(\epsilon) = \left(\frac{\pi}{2}\right)^{1/2} \epsilon'_{0,i} \Delta \left[sign\,(30 - \epsilon'_{0,i}) \, Erf\left(\frac{30 - \epsilon'_{0,i}}{2^{-1/2}\Delta}\right) \right.$$

$$+ Erf\left(\frac{\epsilon'_{0,i} - 2}{2^{-1/2}\Delta}\right) + \left(\frac{\Delta}{2}\right)^2 \left\{ exp\left[-2\left(\frac{\epsilon'_{0,i} - 2}{\Delta}\right)^2\right] \right.$$

$$\left. \left. - exp\left[-2\left(\frac{30 - \epsilon'_{0,i}}{\Delta}\right)^2\right]\right]\right\}$$

(23)

The second basic integral is of the form

$$I_2 = C_2/(2\gamma^2) \int_{MAX\{\epsilon_m, 2MeV/2\gamma\}}^{\epsilon_M} d\epsilon \; \epsilon^{-(\alpha+2)} \; J(\epsilon)$$

(24)

for integrations over the Gaussian part of the cross section and a power law photon field existing over the energy range $\epsilon_m \leq \epsilon \leq \epsilon_M$ with the form

$$n(\epsilon) = K \, \epsilon^{-\alpha}$$

(25)

The constant C_2 in equation (24) has the value

$$C_2 = KW^{-1} \xi_{A,i} \Sigma_d \Delta^{-1}$$

(26)

The other two integrals are those over the high energy nonresonant part of the cross section above 30 MeV. With the cross section $\sigma_{A,i}$ = constant over this energy range as given by equation (16), the relevant integrals

take the form

$$I_3 = (\pi^2 \hbar^3 c^3)^{-1} D \sigma_{A,i} \left[\int_{\frac{30}{2\gamma}}^{\infty} \frac{\epsilon'^2 d\epsilon}{e^{\epsilon/kT}-1} - \left(\frac{30}{2\gamma}\right)^2 \int_{\frac{30}{2\gamma}}^{\infty} \frac{d\epsilon}{e^{\epsilon/kT}-1} \right] \qquad (27)$$

for a thermal photon spectrum $n(\epsilon)$ and

$$I_4 = K \sigma_{A,i} \left[\int_{MAX\{\epsilon_m, \frac{30}{2\gamma}\}}^{\epsilon_M} d\epsilon \ \epsilon^{-\alpha} - \left(\frac{30}{2\gamma}\right)^2 \int_{MAX\{\epsilon_M, \frac{30}{2\gamma}\}}^{\epsilon_M} d\epsilon \ \epsilon^{-(\alpha+2)} \right] \qquad (28)$$

in the case of a power law photon spectrum.

Equations (27) and (28) assume a constant cross section for all ϵ' above 30 MeV. In reality, photopion production becomes important above 150 MeV and changes the shape of the cross section. However, because of the steeply falling nature of the photon spectrum at high energies, these effects are not important for nuclei with Lorentz factors below 10^{11} (energy per nucleon below 10^{11} GeV).

Equation (14) was evaluated numerically using the above formulas in conjunction with the data given in Tables 1 and 2. Photodisintegration rate for nuclei with atomic mass numbers up to 56 were thereby evaluated. (For the three nuclei ^{3}He, ^{4}He and ^{9}Be with nonresonant channels having large values of Δ ($\Delta \gg$ 10 MeV), the 30 MeV cutoff formalism was not employed.)

Figures 4 through 6 show samples of the results obtained giving $R_{A,i}^{-1}$ as a function of γ. It is interesting to note how the width of the low energy

part of the cross section Δ affects the rate calculations for $\gamma \sim 3 \times 10^9$.

Another important effect is the difference in the energy dependence between the reaction channels dominated by the giant resonance (i = 1,2) and those channels which only contribute to the high energy part of the cross section. By combining the rates from all the reaction channels for a given nucleus, the effective nucleon loss rate for the nucleus can be calculated from the relation

$$R_{eff,A} = (dA/dt) = \sum_i iR_{A,i} \tag{29}$$

The quantity $R_{eff}^{-1}(\gamma)$ is shown in Figure 7 for ^{56}Fe along with the single emission timescale $R_{56,1}^{-1}$ in order to demonstrate the importance of multinucleon emission processes in determining the effective nucleon loss rate.

The different energy loss rates for nuclei can now be compared. Figure 8 the characteristic energy loss timescale $\tau_E = (dE/dt)^{-1}E$ for ^{56}Fe from the effect of redshift losses, photodisingtegration and pair production losses. The photodisintegration timescale is shown for both the LIR and HIR cases. It can be seen that for ^{56}Fe , the energy loss rates from pair production and photodisintegration are comparable in the energy range near 10^{20} eV.

For photodisintegration, the average fractional energy loss rate

$$E^{-1}(dE/dt) = A^{-1}(dA/dt) \tag{30}$$

because the nucleon emission is isotropic in the rest system of the nucleus. The Lorentz factor, which is equivalent to energy per nucleon, is conserved for photodisintegration as opposed to the pair production and photopion production processes which involve the creation of new particles which carry off energy.

The energy loss time for pair production $\tau_{E,pp} \propto AZ^{-2}$ as implied by equation (4) which increases $\sim A^{-1}$. The energy loss time from photodisintegration implied by equation (30) is almost independent of A. Thus, the relative importance of pair production as an energy loss process vis-à-vis photodisintegration decreases with decreaing Z when we consider nuclei lighter than iron.

5. Monte Carlo Calculations of the Photodisintegration Histories of Nuclei.

As can be seen from the results of the previous section, the photodisintegration rates for all nuclei have typically steep γ dependences. Pair production can also be quite sensitive to γ. Photodisintegration conserves γ but pair production losses continually and cumulatively act to decrease the value of γ thereby directly affecting the photodisintegration rate. Thus, after a given period of time nuclei with the same initial value of γ aquire differing new values of γ depending on their individual disintegration histories A(t) due to the interplay of the differing energy loss processes. The only way to take correct account of the effect of changes in γ and A with time is to keep track of each individual nucleus as it cascades down in A. This is especially important for the low infrared (LIR) case.

These considerations lead us to use a Monte Carlo technique to compute the behavior of nuclei starting at various initial values of γ (designated by γ_0. At each step, each nucleus followed in the calculation is characterized by the two quantities A_k and γ_k (k being the step number). For a given time step, the probability of each reaction A_k going to $A_k - i$ can be calculated using the rates computed previously as functions of γ. The step size Δt is

chosen so that the sum of the probabilities for all possible i is smaller than 1, the difference from unity being the probability for no interactions in a time Δt. Since photodisintegration conserves γ, the new value of γ is then computed for each nucleus using the pair production rate.

Using the Monte Carlo technique, for each step we randomly determine the reaction channel for each nucleus in the system by assigning a random number to the nucleus and associating the occurrance of a particular channel with a set of such numbers such that the size of the set is proportional to the branching ratio for that channel. The Principle of Large Numbers then states that, given enough nuclei in the system considered, the frequency of random occurrances followed in the calculation will reflect the true probability distribution of the reactions as determined by their branching ratios.

The complete photodisintegration of iron takes, on the average, about 20 events if one includes multinucleon channels, which indicates that choosing a computation run involving a few hundred time steps corresponds to a small interation probability for each step. The total number of particles in the system must also be such that the number of particles having a value A' near $<A>$ at a given time t is large enough so that a fair representation of the branching ratios of different reaction channels can be obtained after they all undergo one interaction.

For each inital value γ_0 used in a computation run, 500 particles were followed in the photodisintegration cascade. The partial results of two such runs are shown in Figure 9 which shows the cumputed histories of two beams of ^{56}Fe nuclei staring out at different initial energies. For comparison, we also

indicate in the figure the lifetime for ^{56}Fe against one nucleon loss for each initial energy. These runs were made using the HIR case and it is quite obvious that, even in this case, the lifetime for complete photodisintegration of iron is $\sim$200 times higher than for the single nucleon loss process. Figure 10 shows the computed values of $<\gamma(t)>$ for various values of γ_0 for ^{56}Fe. Also shown for comparison is the function $\gamma(t)$ for energy loss of protons from pair production for one typical value of γ_0.

In a few test cases, the same cascade was run several times with a different set of random numbers and different values of Δt. Typical differences in $<A>$ introduced by such changes were of the order of $\lesssim$ 1 percent. This proved that the number of particles and time steps used in the computation yielded results with adequate precision.

Using the computed values of the functions $<A(t)>$ and $\gamma(t)$ obtained for different initial energies, the effect of photodisintegration on a power law initial energy distribution can be calculated. This procedure is preferable to the introduction of a power law distribution in energy of the nuclei used in a Monte Carlo run in which case poorer results are obtained because in that case inefficiencies would result from there being either too many or too few particles in some energy ranges due to the steepness of the initial spectrum.

For comparison with the results of the Monte Carlo calculation, the quantity dA/dt for ^{56}Fe shown in Figure 7 can be used together with the approximation that the photodisintegration cross section scales like $NZ/A \simeq A/4$. Thus, for the HIR case for which photodisintegration is significantly more important

than pair production [1]

$$\left.\frac{dA}{dt}\right|_A \simeq \left.\frac{dA}{dt}\right|_{Fe} \left(\frac{A}{56}\right) \tag{31}$$

which implies that A(t) is an exponential function of time with an e-folding

time of $56(dA/dt)^{-1}_{Fe}$. Figure 11 shows the function $<A(t)>$ obtained from the

Monte Carlo calculations for various γ_0. for both the HIR and LIR cases. We

also show for comparison the value of A(t) obtained under the approximation

given by equation (31). In the HIR case, A is not decreasing as fast as the

simple scaling approximation (31) would imply because of the diminishing rel-

ative importance of multinucleon channels for lighter nuclei. For the LIR

case it is apparent that more than just a change in the photodisintegration

rate is occurring because of the definite change in the character of the func-

tion A(t) for $t \gtrsim 5 \times 10^{15}$ s. This change is due to the effect of pair prod-

uction on γ which can be seen to be qualitatively more than a small correction

and illustrates the rationale for using the Monte Carlo method in order to ob-

tain results which are truly valid. The shaded areas around the curves shown

in Figure 11 show the one standard deviation spread in A around $<A>$ determined

from the Monte Carlo computations from more detailed information as illustrated

in Figure 9. More $<A(t)>$ curves are shown in Figure 12. By combining these $<A(t)>$

results with those on $\gamma(t)$ for various values of γ_0, one can obtain the function

$<A(\gamma_f)>$ where γ_f is the final value of γ for nuclei starting out as Fe after some

time t when they have disintegrated to nuclei of mass A. This function for vari-

ous values of t is shown in Figure 13.

---

[1] The actual dependence of the photodisintegration cross section on A is somewhat
higher as can be seen from the values of ξ given in Table 1.

6. Astrophysical Implications of the Results.

The results of the Monte Carlo computations discussed in the previous section can be used to discuss the effect of photonuclear emission processes on ultrahigh energy nuclei in intergalactic space by evaluating their effect on an initial beam of ^{56}Fe nuclei with a power law energy spectrum at injection. One may then ask how this energy spectrum changes after a given period of time corresponding to the mean age of the nuclei under various assumptions as to their origin. The predicted characteristics of the ultrahigh energy cosmic rays under these various assumptions may then be compared with the data regarding the energy spectrum of ultrahigh energy cosmic rays given in terms of total energy per nucleus from air-shower observations.

We shall consider here two hypotheses of particular astrophysical significance, viz., the universal origin hypothesis and the local supercluster origin hypothesis. For the universal origin hypothesis, we can consider that cosmic rays have been produced at a roughly uniform rate throughout a time t_H which is related to the Hubble constant H_0 and given by $(2/3)H_0^{-1}$ for an Einstein-de Sitter universe and H_0^{-1} for a low density universe where H_0 is taken to be 50 km$\cdot$s$^{-1}\cdot$Mpc. The average age of the cosmic rays is then $t_H/2$.

For the supercluster origin hypothesis, we assume that most of the cosmic rays we observe at ultrahigh energy are produced within the local supercluster of galaxies which is centered on the populous Virgo cluster at a distance of $\sim$ 20 Mpc and of which our Galaxy is considered to be a member. Under this hypothesis, the average age of the ultrahigh energy cosmic rays will be $\sim2\times10^{15}$ s.

Of course, an equilibrium spectrum of such cosmic rays produced from a uniform distribution of sources will contain a spread in values of A at a given value of γ. Nevertheless, the functions shown in Figures 11 and 12 giving A(t) show that a dispersion of a factor of 2 in the age introduces a dispersion in A which is not larger than the dispersion introduced by the cascade process itself. To simplify the discussion we shall first consider the time behavior of a power law energy spectrum of Fe nuclei injected in a burst at an initial time t = 0. Starting with such an initial spectrum $J(\gamma_0)$ and knowing $\gamma_f(t)$ and A(t), there are then two well defined functions $\gamma_f(\gamma_0)$ and $A(\gamma_f)$. This is because the change in γ with time is determined by the pair production and redshift energy loss rates and the photodisintegration process changes A without changing γ. The spectrum in γ_f at time t is is then obtained from the inverse function $\gamma_0(\gamma_f)$ using the relation

$$I(\gamma_f ; t) = (\gamma_0/\gamma_f) J\{\gamma_0(\gamma_f)\} \qquad (32)$$

The final energy of the nuclei is, of course, $E = \gamma_f A(\gamma_f) m_p$. $E(\gamma)$ is a non-monotonic function which reaches a maximum at a critical energy E_c, then decreases again to a minimum and starts increasing again with γ. This implies that nuclei having an energy $E = E_c + \delta E$ must have started out with an initial γ_0 much larger than those having an energy E_c because of the rapid change of A with γ from photodisingtegration. Naturally, those nuclei having started out with a much higher value of γ_0 were produced with a much lower intensity. The physical result of this is then that there is a resultant discontinuity or effective cutoff in the predicted equilibrium spectrum at an energy E_c. In reality, the cutoff will not be infinitely sharp because of the dispersion in A as-

sociated with the cascade (see, e.g., Figure 11) and the dispersion in age of

the cosmic rays due to the spatial distribution of the sources. Nonetheless,

there will be a sharp drop in the cosmic ray intensity near the value of E_c

associated with the mean age of the cosmic rays.

Starting with an injection spectrum $J(\gamma_0) \propto \gamma_0^{-3}$, the resultant spectrum

$I(E;t)$ was calculated for various values of t associated with the universal

origin and supercluster origin hypotheses. The function $E^3 I(E;t)$ is plotted

in Figure 14 for the HIR case and in Figure 15 for the HIR case, given in

arbitrary units. By comparison, the observational data on the energy spec-

trum $E^3 I(E)$ as given by Hillas (1974) are consistant with a straight horizon-

tal line ($I(E) \propto E^{-3}$) up to the highest observed energy of $\sim 2 \times 10^{20}$ eV.

The value of E_c given as a function of time is shown in Figure 16.

From this figure, it can be seen that a typical dispersion in cosmic ray

age of a factor of 2 will produce a change in E_c by less than a factor of

2 so that the predicted cutoff energy as a function of cosmic ray age is

quite well defined. Thus, the low cutoff energy predicted for the universal

cosmic ray hypothesis on the assumption that the initial cosmic rays are

intermediate mass nuclei is in clear contradiction with the observations.

In the case of the supercluster hypothesis however, the predicted cutoff

energy is too close to the upper limit of the observations, especially con-

sidering the error involved in determining the energy of a shower-producing

particle in the 10^{20} eV range, to imply any contradiction. Although the re-

sults shown in Figures 14 and 15 are given for an initial composition of ^{56}Fe,

the values of E_c for nuclei of lower $<A>$ will be even lower because $E \propto A$ for

a given value of γ and the characteristic energy loss rate from photodisinte-

gration is almost independent of A at a given value of γ.

The secondary nucleons produced in the photodisintegration reactions, which eventually become protons, are emitted isotropically in the rest frame of the parent nuclei and thus have, on the average, the same Lorentz factor as the parent. These secondaries lose energy through pair production and photomeson production interactions at a rate which is slower than that of the parent nuclei. Nevertheless, for a given value of γ_0 such that γ_f is a fairly good approximation for the average γ of the secondaries. The spectra of the secondaries obtained under this approximation are shown in Figures 14 and 15 assuming no cutoff in the injection spectrum. For energies above E_c, for which the secondaries are dominant, the value of γ_0 associated with their parent primaries is very large and the associated value of A has been 1 for most of the time considered, making our approximation a good one. It can be seen that the existence of a secondary proton component does not affect our prediction of a sharp cutoff in the observed spectrum at E_c.

7. Conclusions.

The results of this paper clearly indicate that ultrahigh energy cosmic rays therefore cannot be universal in origin <u>regardless of whether they are</u> <u>protons or nuclei</u>. (The cutoff energy for protons can be seen from Figure 2 to occur at $\sim 5 \times 10^{19}$ eV due to photomeson production losses with a lower energy steepening predicted to occur at $\sim 2 \times 10^{18}$ eV due to pair production.). Both the supercluster and galactic origin hypotheses, however, are possible for protons (Stecker 1968) <u>and higher mass nuclei.</u>[2]

These conclusions are further supported by reports of a distinct anisotropy in the arrival directions of cosmic rays with energies above 10^{19} eV (Krasilnikov et al. 1974) again arguing against a universal origin for these cosmic rays since a universal origin implies large-scale isotropy.

When measurements of the mean mass of cosmic rays in the 10^{17} to 10^{19} eV energy range become available, the results given here for $A(\gamma_f)$ as shown in Figure 13 can be used to help determine their age and origin further. Should it be found in the future that the cosmic ray spectrum continues to values of total energy much in excess of 10^{20} eV, this would rule out their being of mixed or intermediate mass composition or of intermediate mass origin even under the supercluster origin hypothesis.

---

[2] Using new estimates of the infrared radiation field in the inner galaxy, as well as estimates of the galactic optical photon field, it can be shown that photodisintegration of nuclei travelling typical galactic distances is negligible. For a further discussion of the galactic origin hypothesis for ultrahigh energy cosmic rays, see Stecker(1971) and Syrovatskii (1971).

ACKNOWLEDGMENT:

REFERENCES

Berezinskii, V. S. and Zatsepin, G. T. 1971. Sov. J. Nuc. Phys. 13, 453.

Blumenthal, G. R. 1970. Phys. Rev. D1, 1596.

Chan, K. L., and Jones, B. J. T. 1975. Astrophys. J. 195, 1.

Clark, T. A., Brown, L. W. and Alexander, J. K. 1970, Nature 228, 847.

Danos, M. and Fuller, E. G. 1965, Ann. Rev. Nuc. Sci. 15, 29.

Field, G. 1972, Ann. Rev. Astr. and Astrophys. 10, 227.

Gorbunov, A. N. 1968, Phys. Lett. 27B, 436.

Greisen, K. 1966, Phys. Rev. Lett. 16, 748.

Hayward, E. 1970, Nat'l. Bureau of Standards Monograph No. 118.

Hegyi, D. J., Traub, W. A., Carleton, N. P. 1974, Astrophys. J. 190, 543.

Hillas, A. M. 1974, Phil. Trans. Roy. Soc. Lond. A 277, 413.

Hoffmann, W. F., Frederick, C. L. and Emery, R. J. 1971, Astrophys. J. 170, L89.

Houck, J. R., Soifer, B. T., Harwit, M., and Pipher, J. L. 1972. Astrophys. J.
    178, L29.

Kleinman, D. E., and Wright, E. L. 1974, Astrophys. J. 191, L19.

Krasilnikov, D. D., Kuzmin, A. J., Linsley, J. Orlov, V. A., Reid, R. J. O.,
    Watson, A. A. and Wilson, J. G. 1974, J. Phys. A. 7, L176.

Kompaneets, A. S. 1957. Sov. Phys. JETP 4, 730.

Levinger, J. S. 1951, Phys. Rev. 84, 43.

McNutt, D. P., and Feldman, P. D. 1970. Science 167, 1277.

Muellner, D., and Weiss, R. 1973. Phys. Rev. D7, 326.

Neugebauer, G., Becklin, E., and Hyland, A. R. 1971, Ann. Rev. Astr. and
    Astrophys. 9, 67.

Partridge, R. B. 1974, Astrophys. J. 192, 241.

Partridge, R. B. and Peebles, P. J. E. 1967a, Astrophys. J. 147, 868.

Partridge, R. B. and Peebles, P. J. E. 1967b, Astrophys. J. 148, 377.

Peebles, P. J. E. 1971, Physical Cosmology, Princeton Univ. Press, Princeton.

Pipher, J. L., Houck, J. R., Jones, B. W. and Harwit, M. 1971, Nature 231, 375.

Rieke, G. H. and Low, F. J. 1972, Astrophys. J. 176, L95.

Robson, E. I., Vickers, D. G., Huizinga, J. S., Beckman, J. E. and Clegg, P. E. 1974.
    Nature 251, 591.

Schmidt, M. 1971, Nuclei of Galaxies, ed. D. J. K. O'Connell, North Holland,
    Amsterdam p. 395.

Shectman, S. A. 1974, Astrophys. J. 188, 233.

Soifer, B. T., Houck, J. R. and Harwit, M. 1971, Astrophys. J. 168, L73.

Stecker, F. W. 1968. Phys. Rev. Lett. 21, 1016.

Stecker, F. W. 1969, Phys. Rev. 180, 1264.

Stecker, F. W. 1971, Nature Phys. Sci. 234, 28.

Syrovatskii, S. I. 1971, Comm. On Astr. and Space Phys. 3, 155.

Thaddeus, P. 1972. Ann. Rev. Astr. and Astrophys. 10, 305.

Williamson, K. D., Blair, A. G., Catlin, L. L., Hiebert, R. D., Loyd, E. G.,
    Romero, H. V., 1973, Nature Phys. Sci. 241, 79.

Woody, D. P., Mather, J. C., Nishioka, N. S., Richards, P. L. 1975. Phys.
    Rev. Lett. 34, 1036.

Zatsepin, G. T., and Kuz'min, V. A. 1968, JETP Lett. 4, 78.

Zel'dovich, Ya.B., Illarionov, A. F. and Sunyaev, R. A. 1972.
    Zh. E. T. Fiz. 62, 1217.

FIGURE CAPTIONS

Figure 1.   A graph of the function $f(\nu)$ used in equation (4) as defined by

Blumenthal (1970).

Figure 2.   The energy loss time and attenuation length for protons from pair

production, redshift, and photopion production losses based on the

calculations of Stecker (1968) and Blumenthal (1970).   Also shown

is the attenuation length for ^{56}Fe from pair production losses.

Figure 3.   Computed background radiation fields from quasars, Seyfert and

related galaxies and normal galaxies as discussed in the text.

Also shown are the 2.7 K microwave and optical radiation fields

as well as some measured values and upper limits.   The dotted

lines labelled HIR and LIR were taken as alternative models for

the intergalactic infrared background fields used in the cal-

culations.

Figure 4.   Rates for i-nucleon loss from nuclei of mass number A, labelled

$R_{A,i}^{-1}$ in seconds for an appropriate sample showing the effect of

different cross section widths Δ on the shape of $R(\gamma)$.

Figure 5.   more sample inverse rates (see caption for Figure 4).

Figure 6.   More sample inverse rates (see caption for Figure 4).

Figure 7.   The effective inverse nucleon loss rate for ^{56}Fe shown along

with the single emission timescale to demonstrate the importance

of multinucleon emission processes.

Figure 8.   Energy loss time for ^{56}Fe shown for redshift, pair production, and

photodisintegration losses in the HIR and LIR cases.

Figure 9.   Calculated histories of two beams of ^{56}Fe nuclei with two different

initial energies shown for the HIR case.   Also shown in both cases

are ten times the value of the lifetime for Fe against one nucleon

loss. The gap in the distribution for A between 4 and 9 is caused by the reaction $\gamma + {}^9Be \rightarrow 2\alpha + n$. The intensities shown for A = 1 and 4 are underestimated since they do not include the contribution of the secondary products of the photoemission interactions.

Figure 10. The computed value of $\gamma(t)$ for ${}^{56}Fe$ with given initial values γ_0 shown by the solid lines. The dashed line shows the function $\gamma(t)$ for protons with $\gamma_0 = 3 \times 10^9$ for comparison.

Figure 11. Sample values of $<A(t)>$ for two values of γ_0. The HIR case is shown by the solid lines, the LIR case is shown by the dashed line and the scaling approximation (see text) is shown by the dot-dash line.

Figure 12. More sample values of $<A(t)>$. Solid lines: HIR case, dashed lines: LIR case.

Figure 13. The function $A(\gamma_f)$ calculated for various timescales of astrophysical significance. Solid lines: HIR case, dashed lines: LIR case.

Figure 14. Calculated shape of the ultrahigh energy cosmic ray spectrum after a time t from injection of a γ^{-3} primary ${}^{56}Fe$ spectrum given as $E^3 I(E)$ in arbitrary units for the HIR case and astrophysically significant timescales with the effect of secondary protons included.

Figure 15. Calculated shape of the ultrahigh energy cosmic ray spectrum in the LIR case (see caption for figure 14).

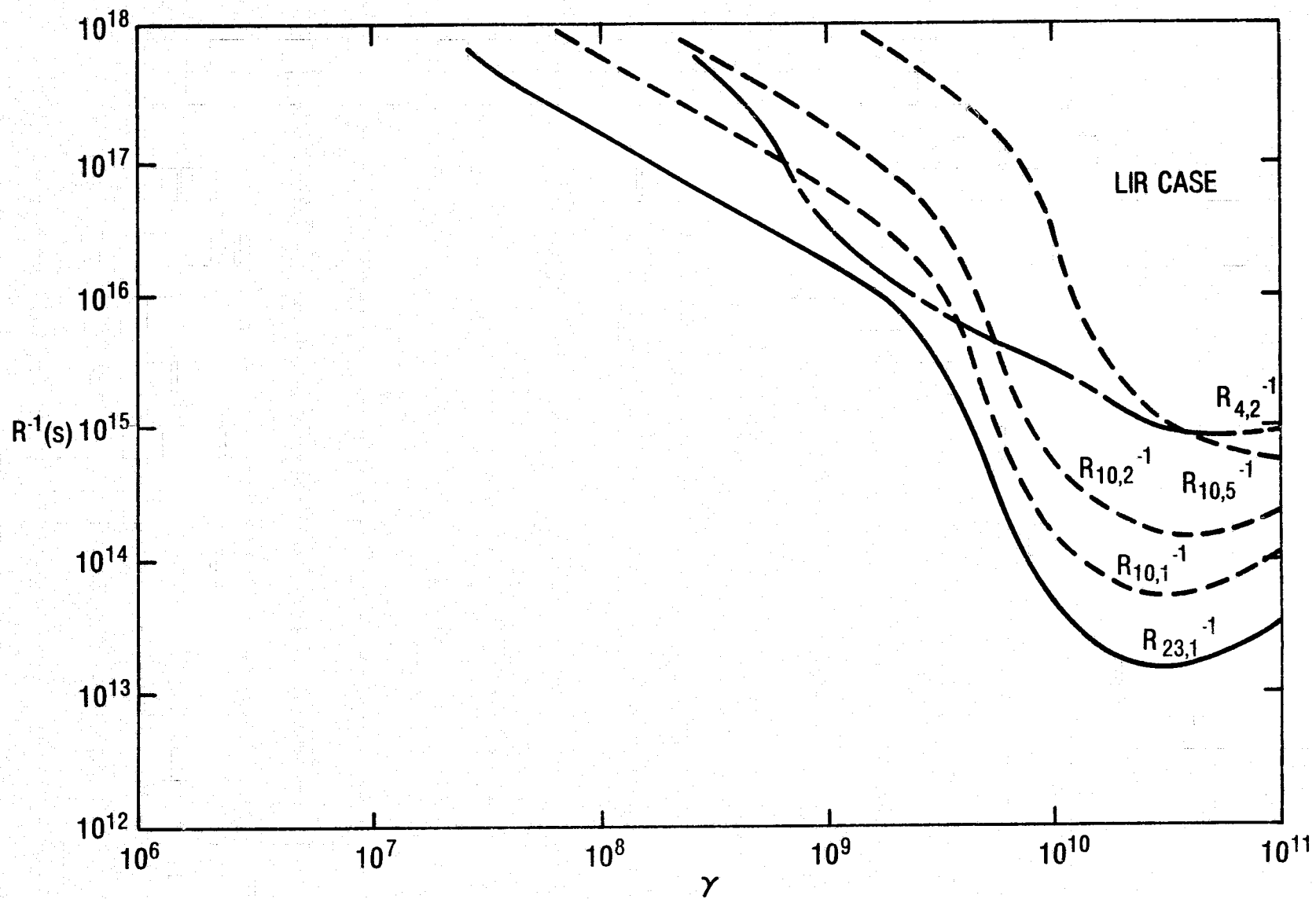Figure 16. Value of the calculated cutoff energy E_c for ultrahigh energy cosmic rays starting out as Fe and evaluated after a time t.

FIGURE 1
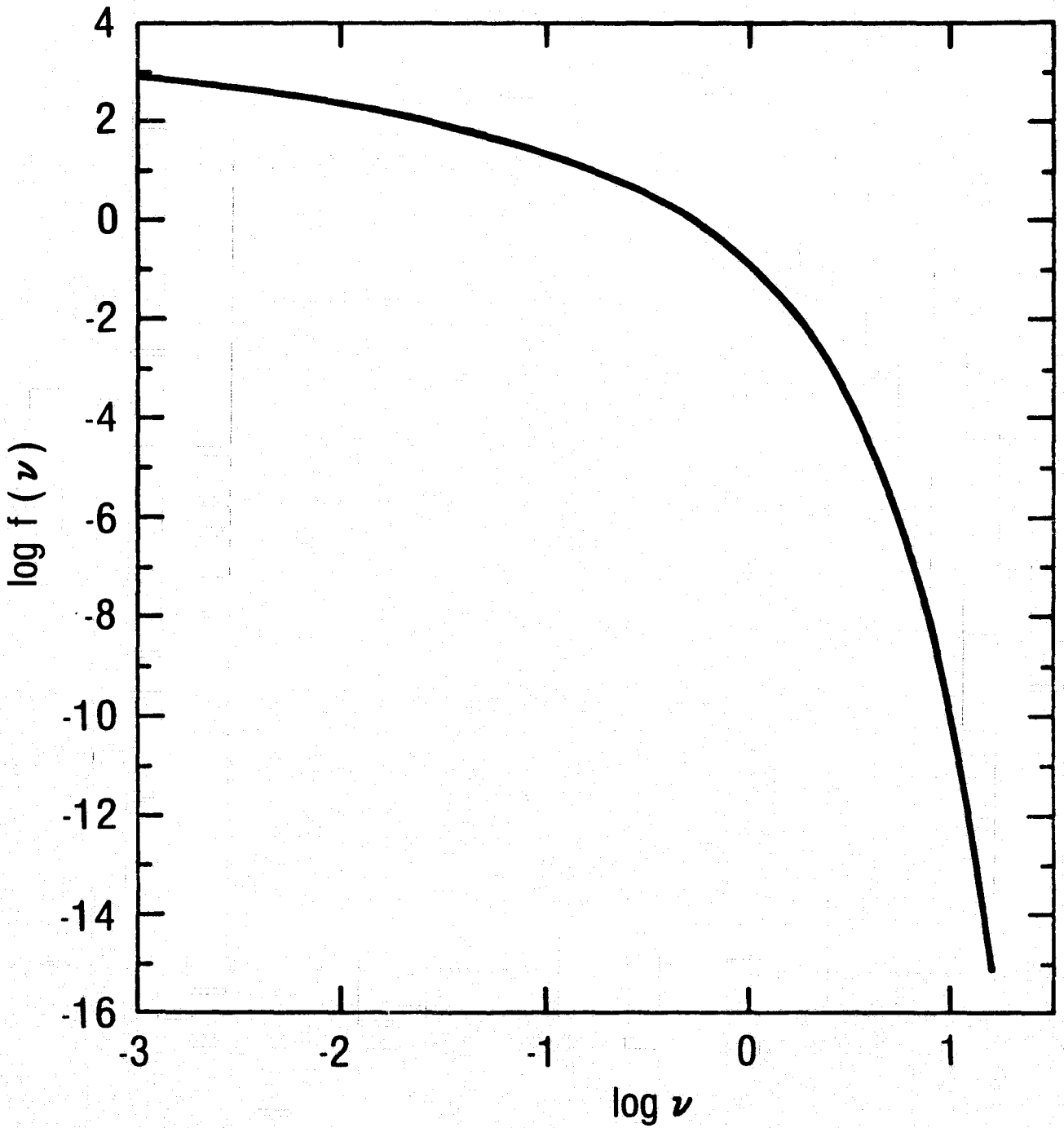
FIGURE 2

FIGURE 3

FIGURE 4

HIR CASE
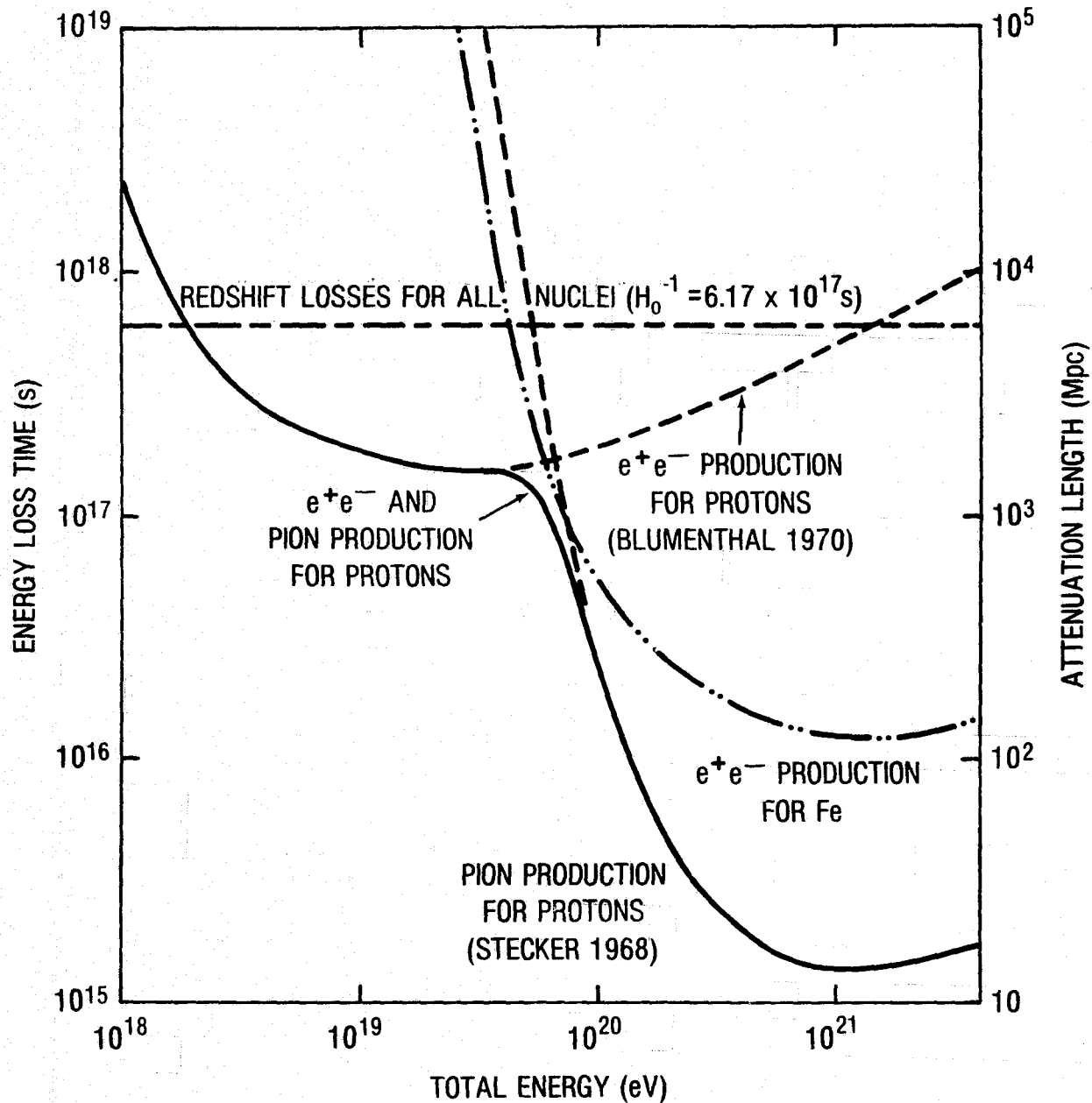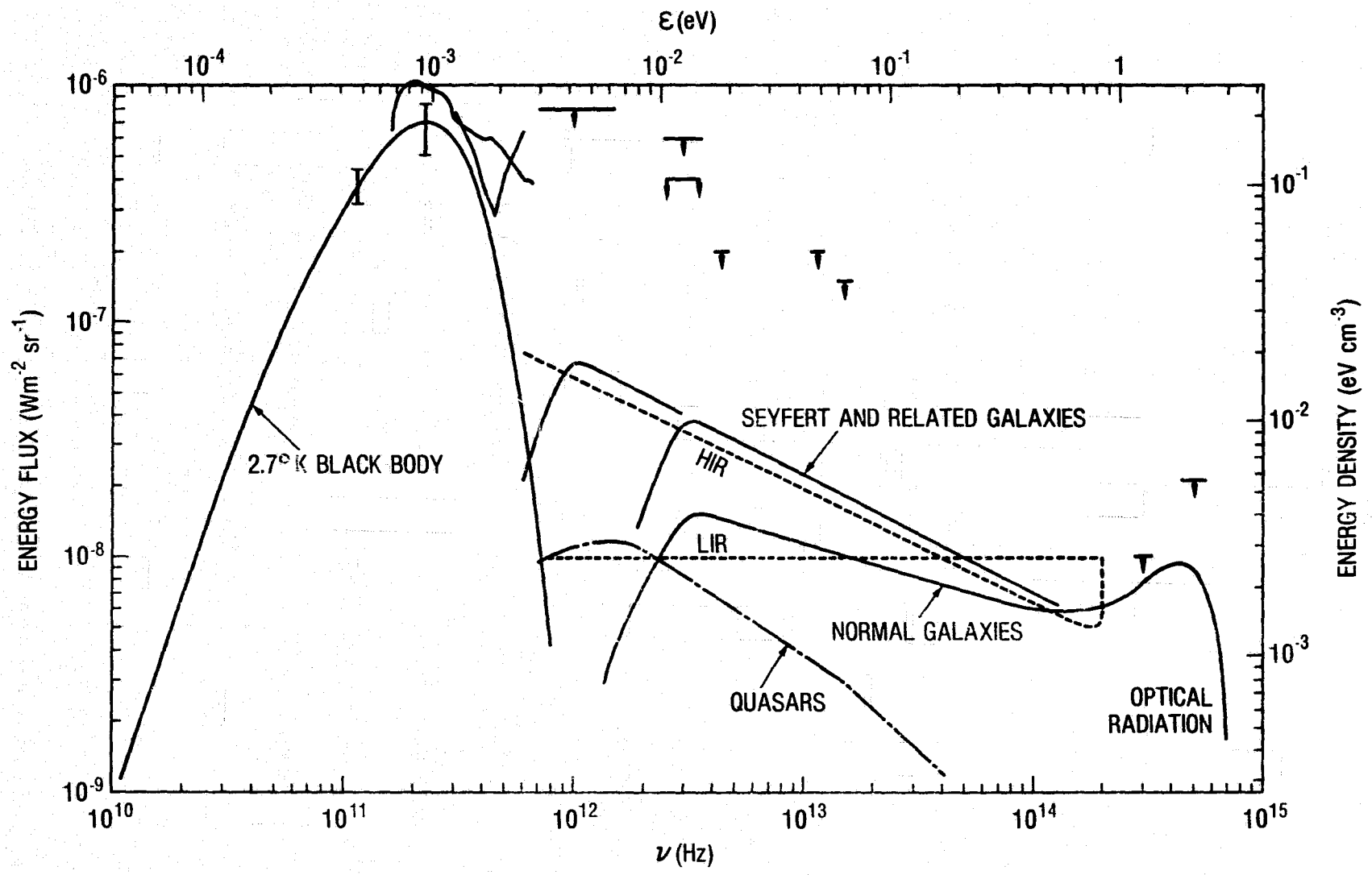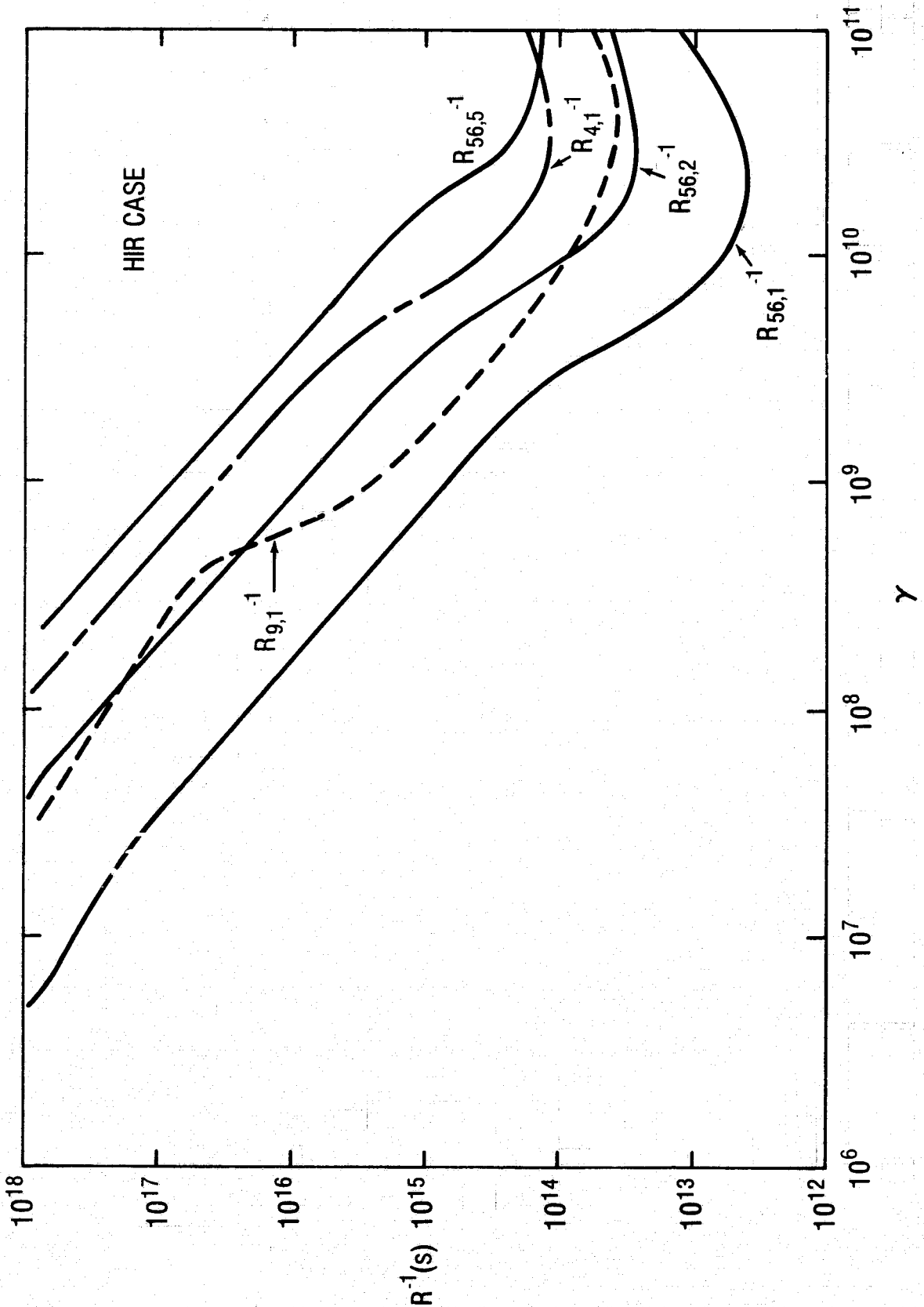
FIGURE 5

FIGURE 6

FIGURE 7

HIR CASE

$R_{56,1}^{-1}$

$R_{eff, 56}^{-1}$

$R^{-1}(s)$

γ

FIGURE 8

FIGURE 9

FIGURE 10

Figure showing $\gamma(t)$ versus t (s) with curves for $\gamma_0 = 10^{10}$, $\gamma_0 = 4 \times 10^9$, $\gamma_0 = 3 \times 10^9$, $\gamma_0 = 10^9$, and $\gamma_0 = 4 \times 10^8$.
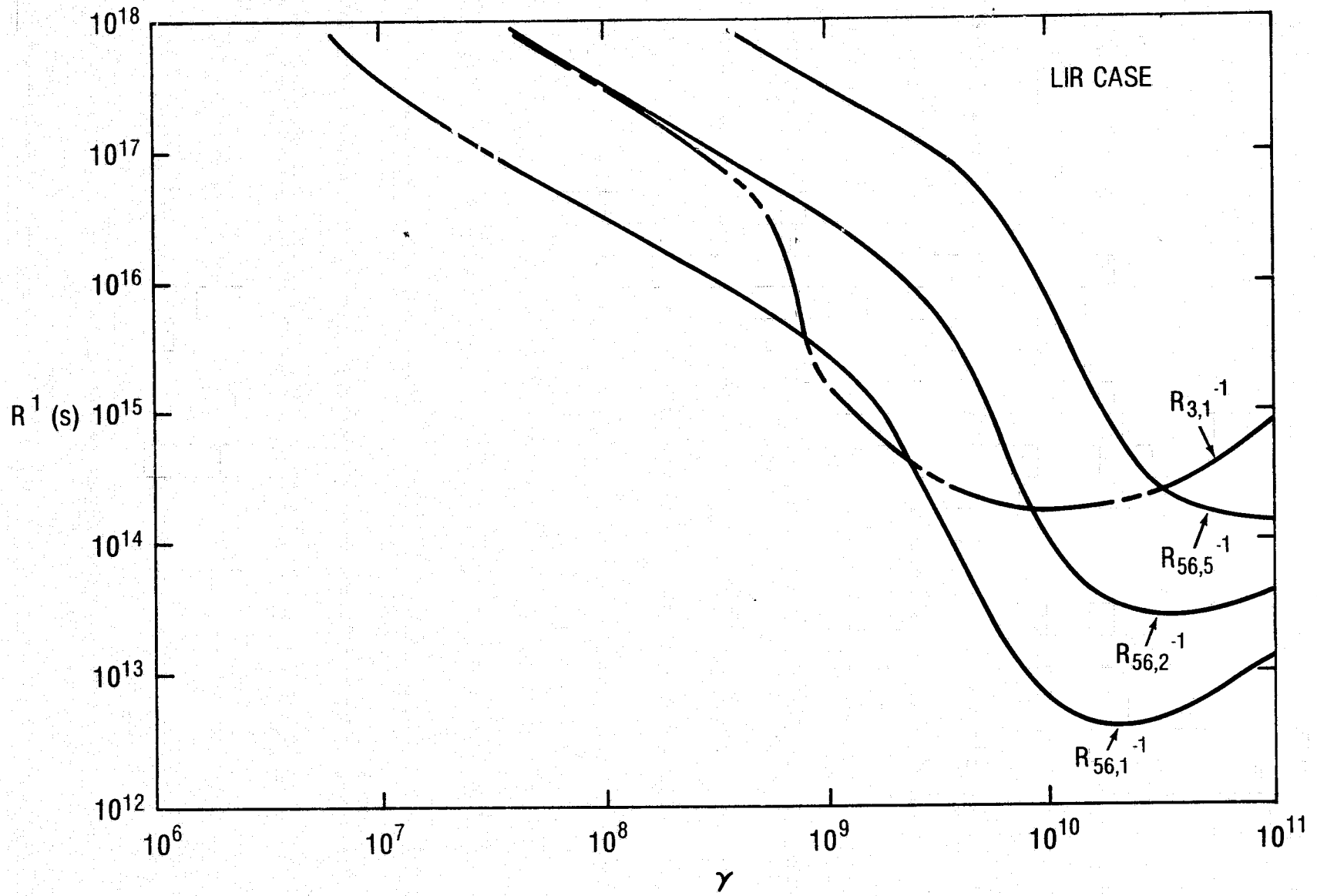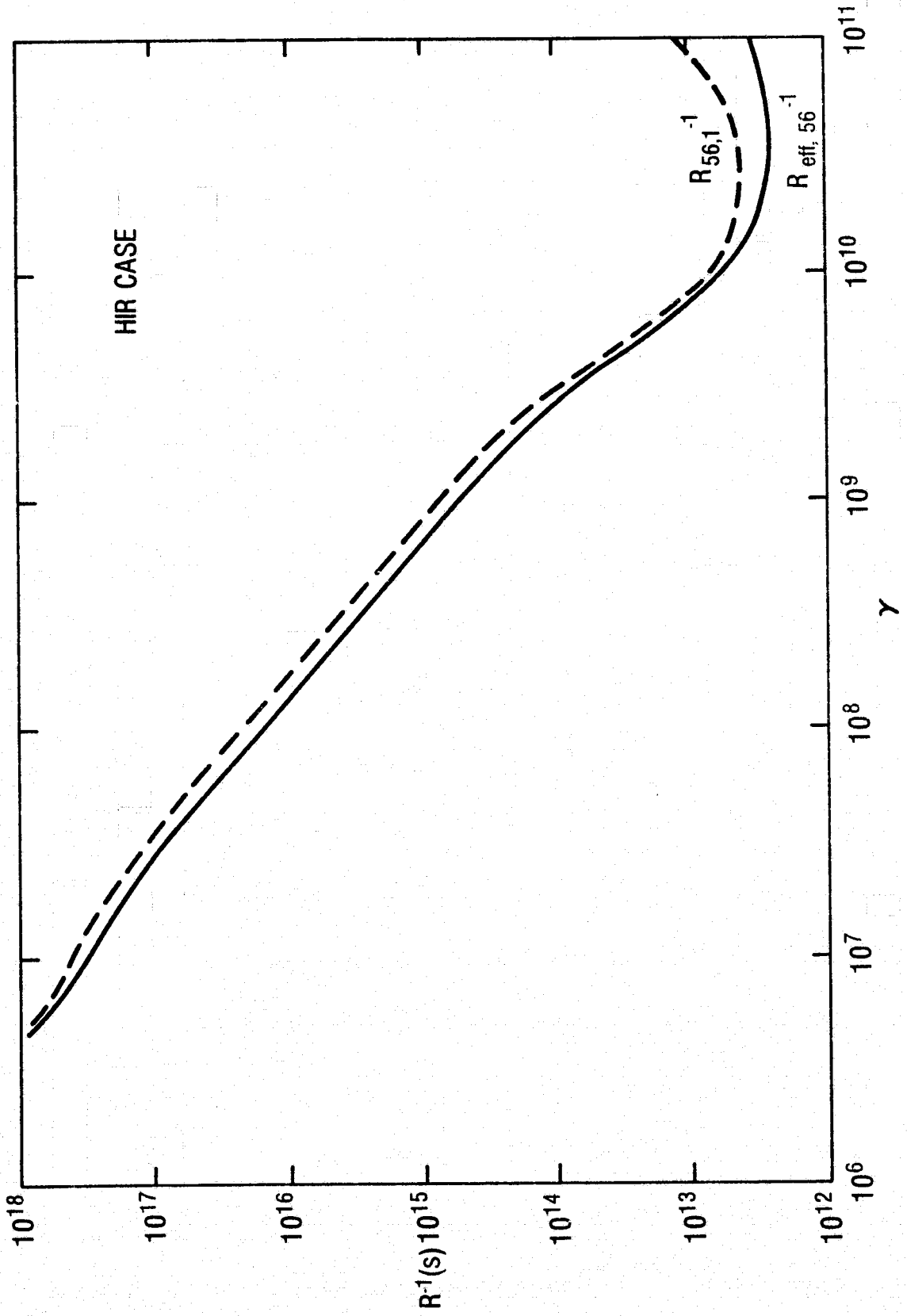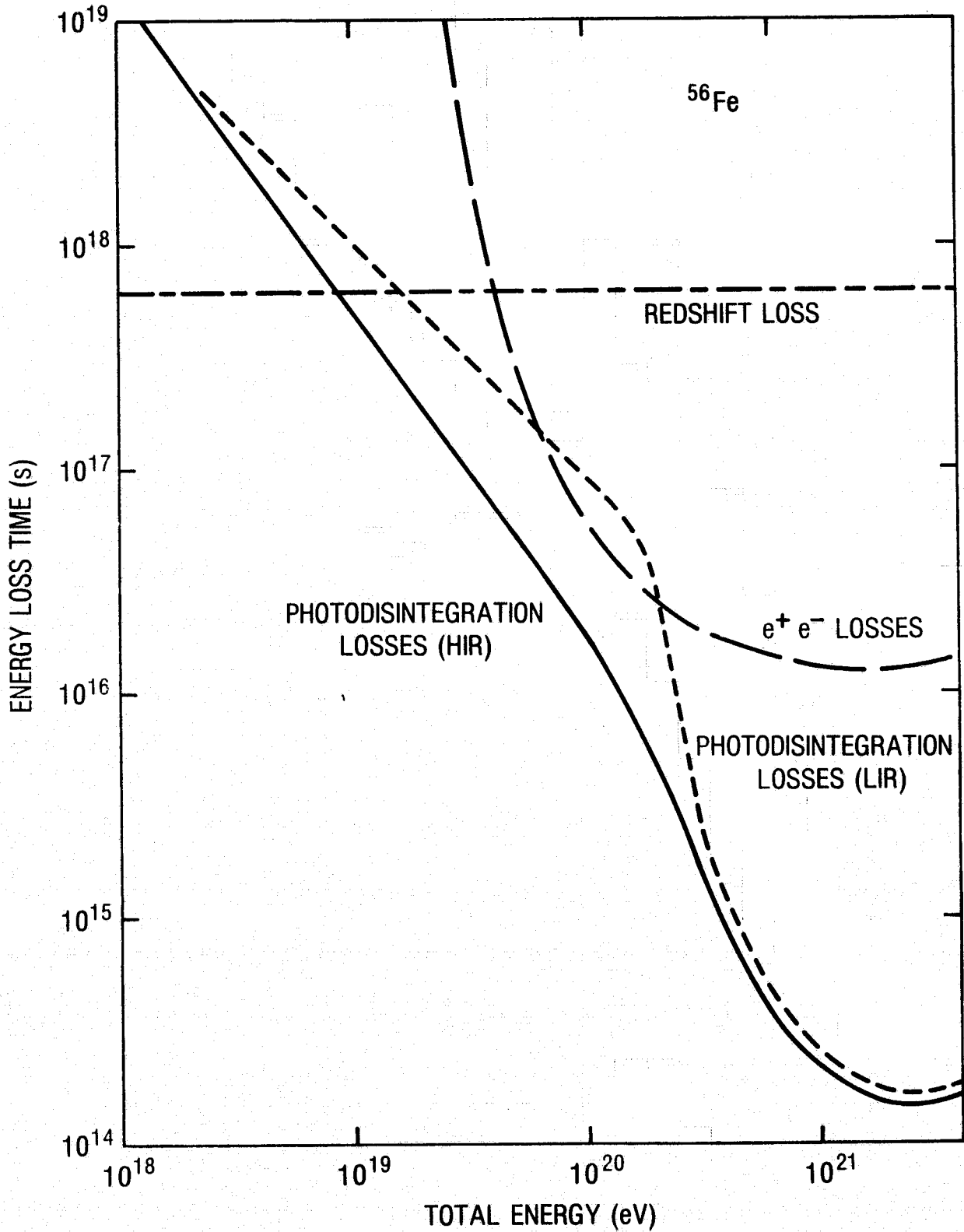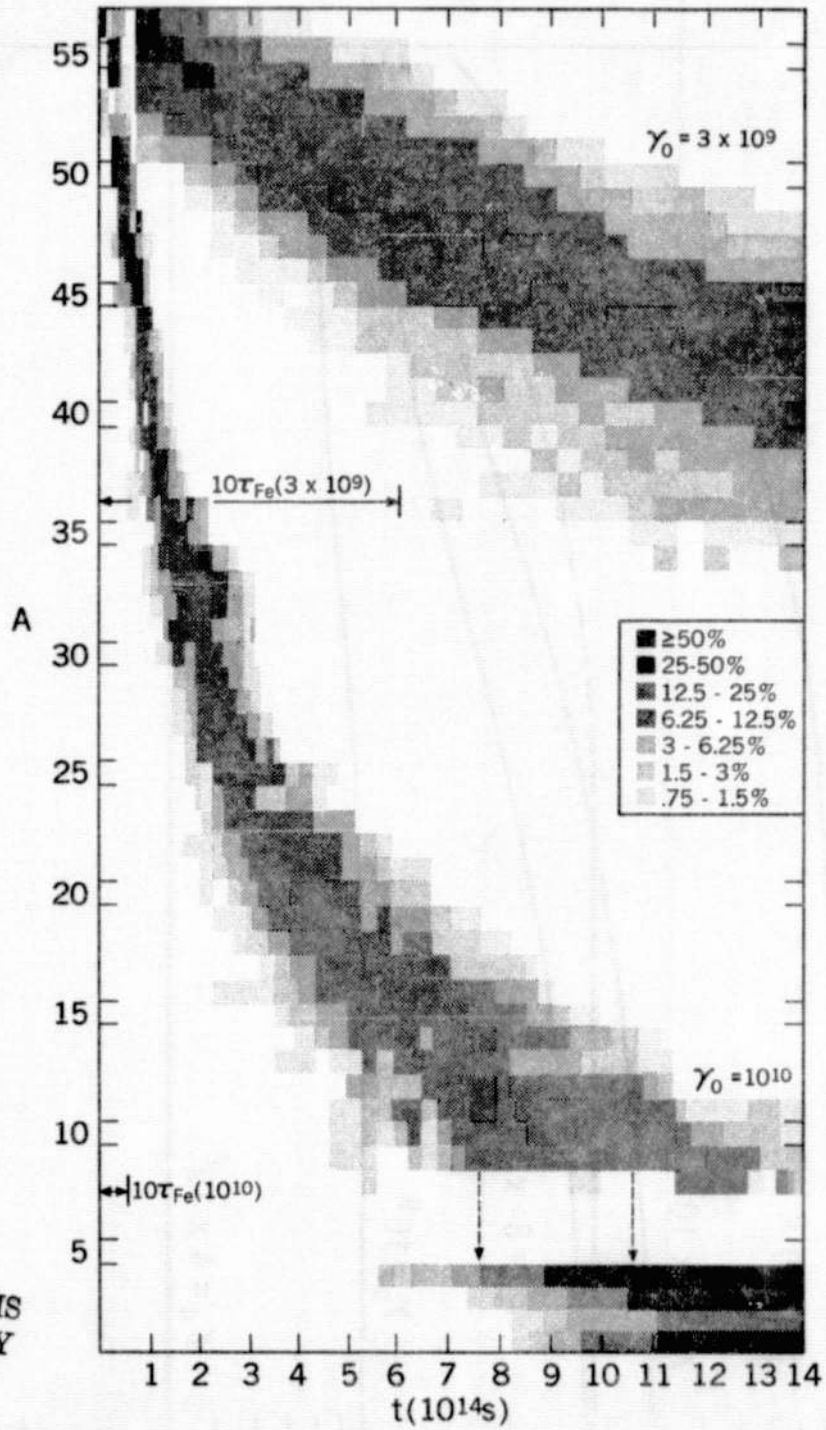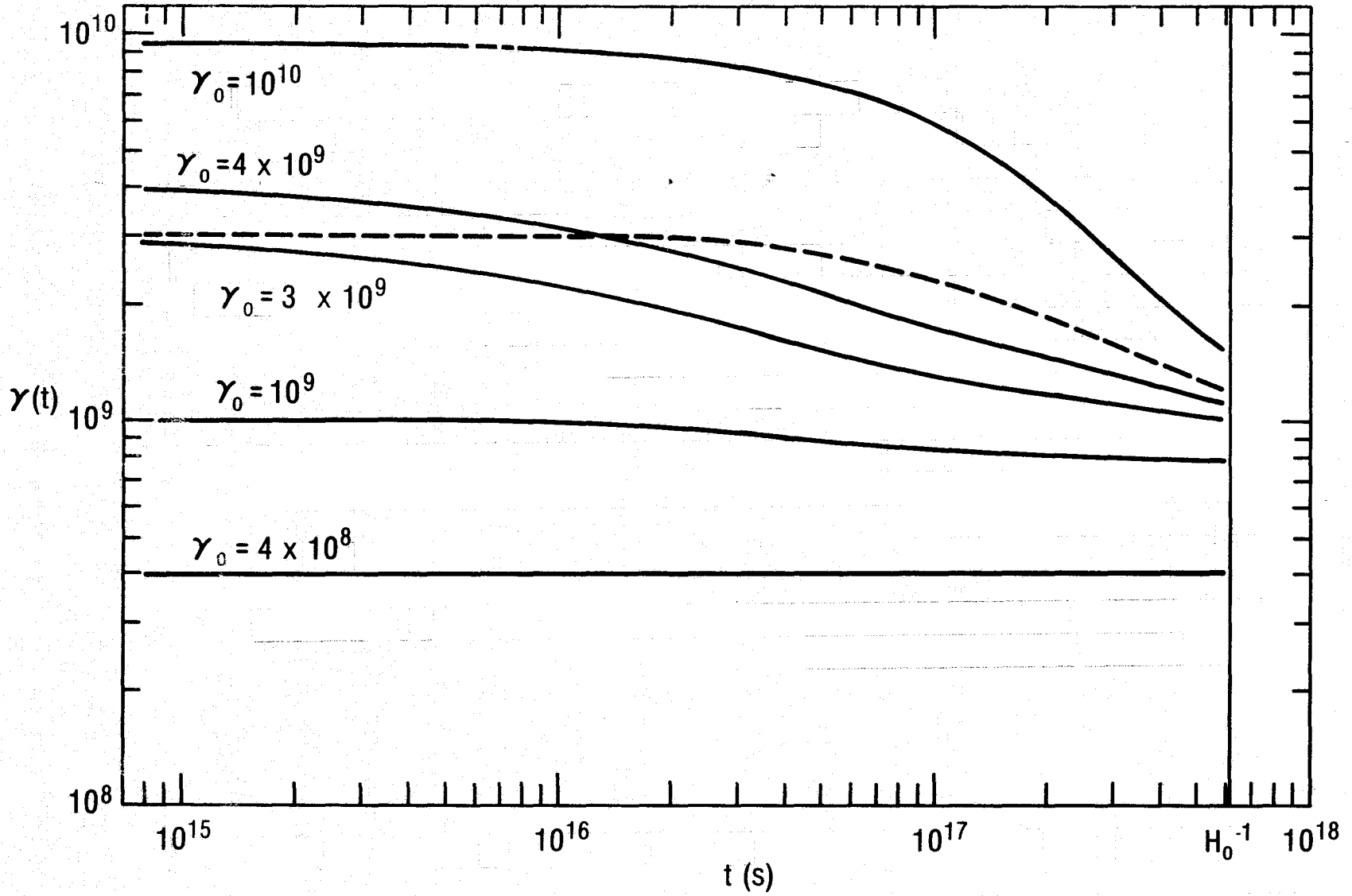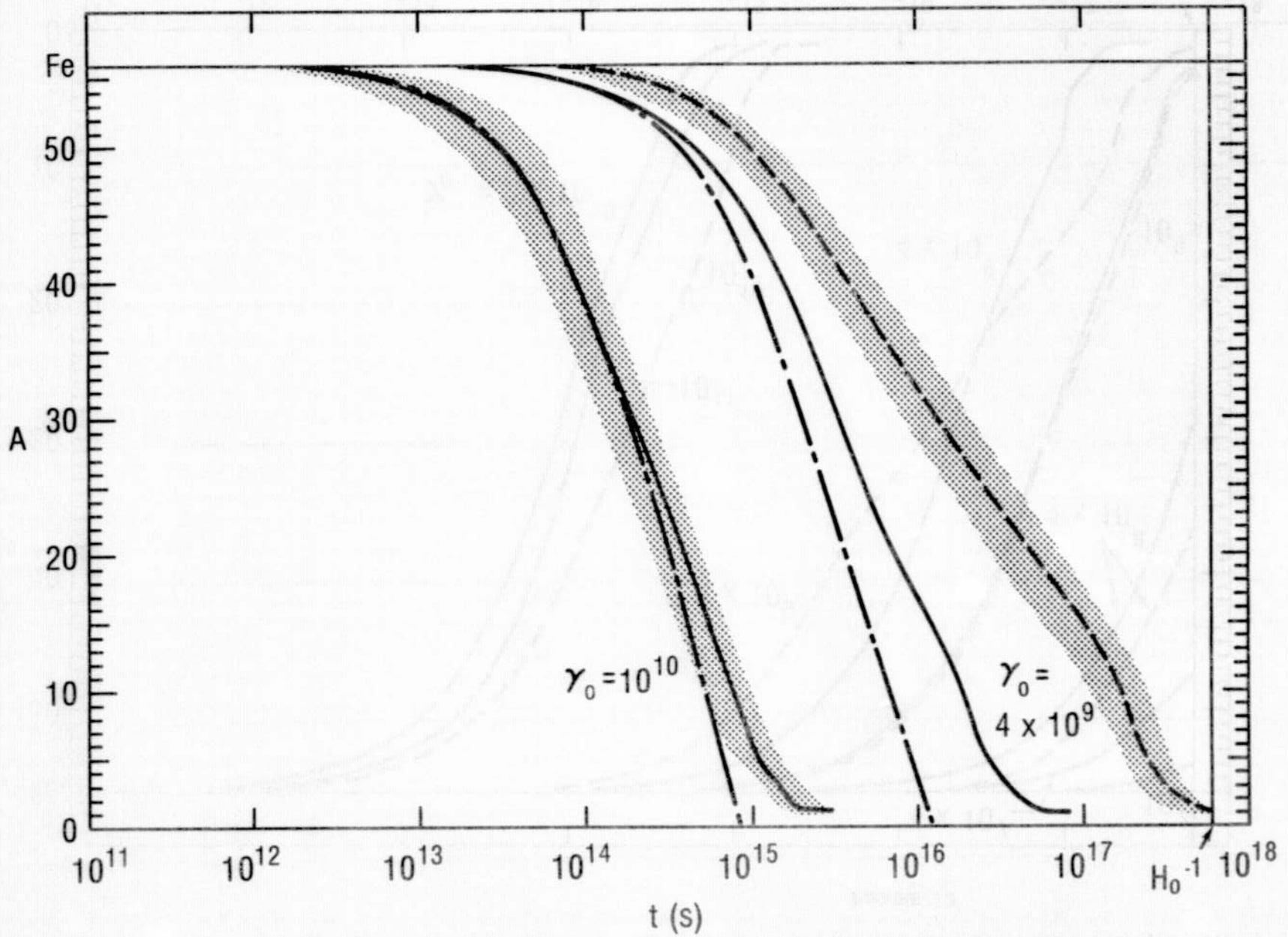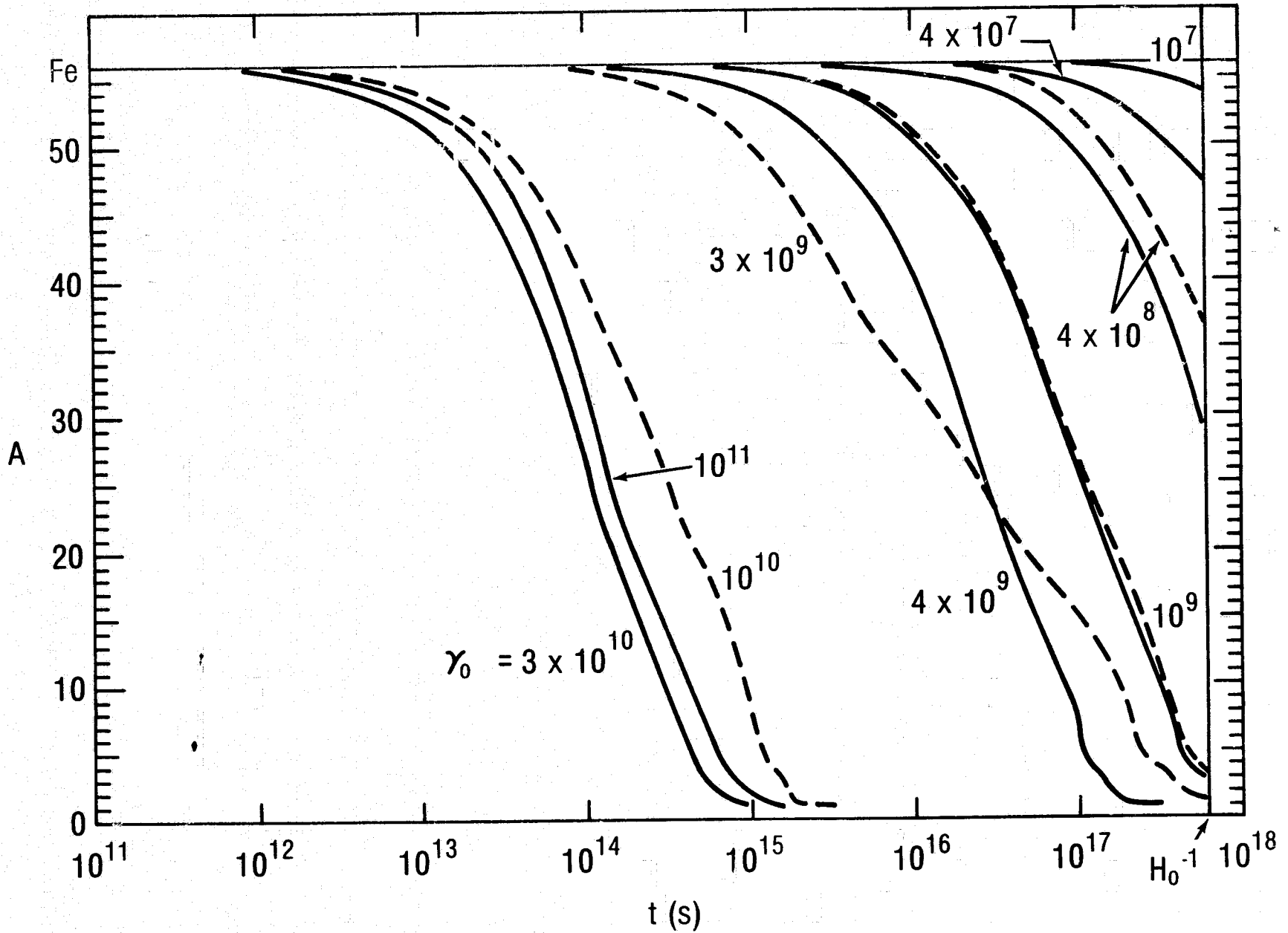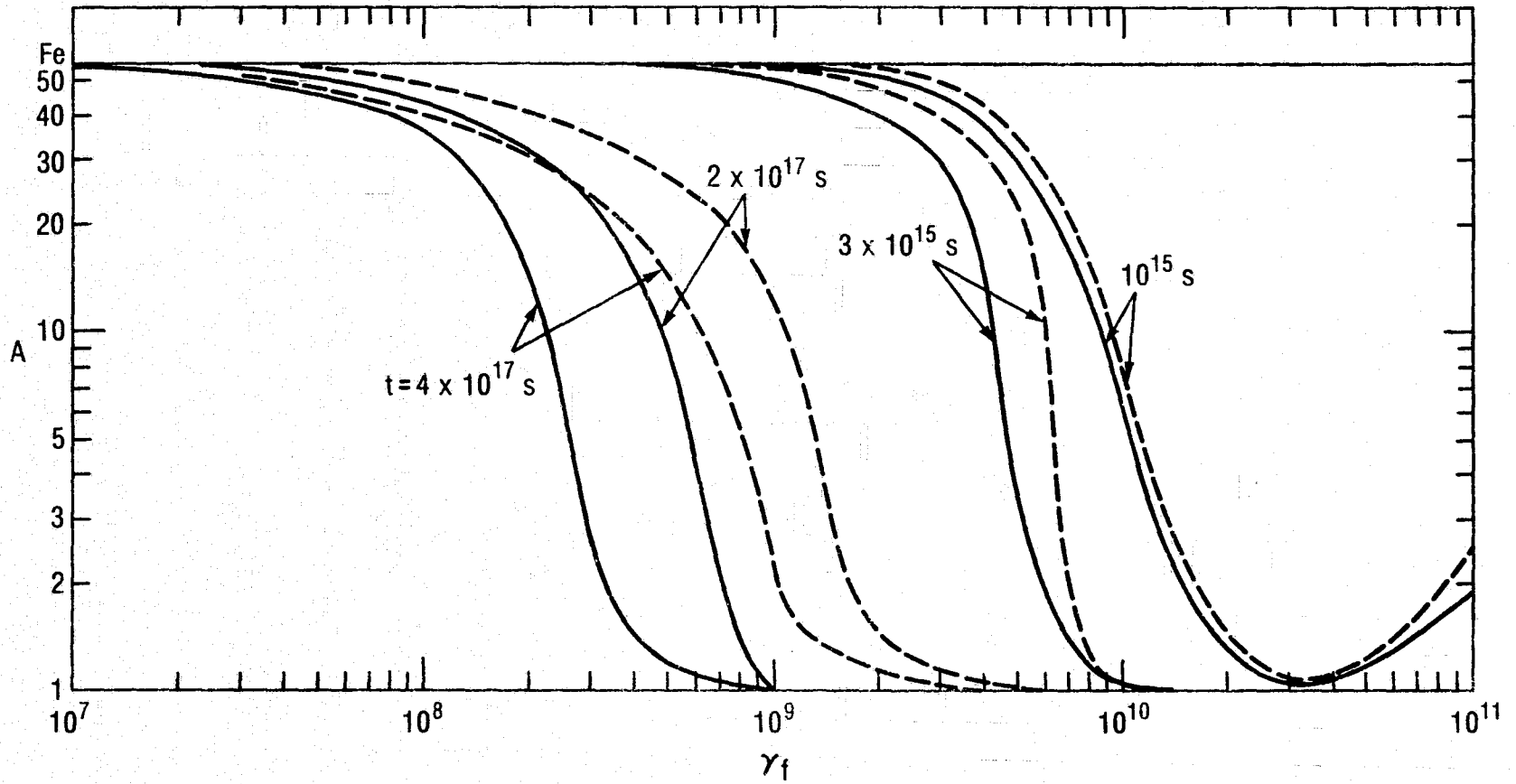
FIGURE 11

FIGURE 12

FIGURE 13

FIGURE 14
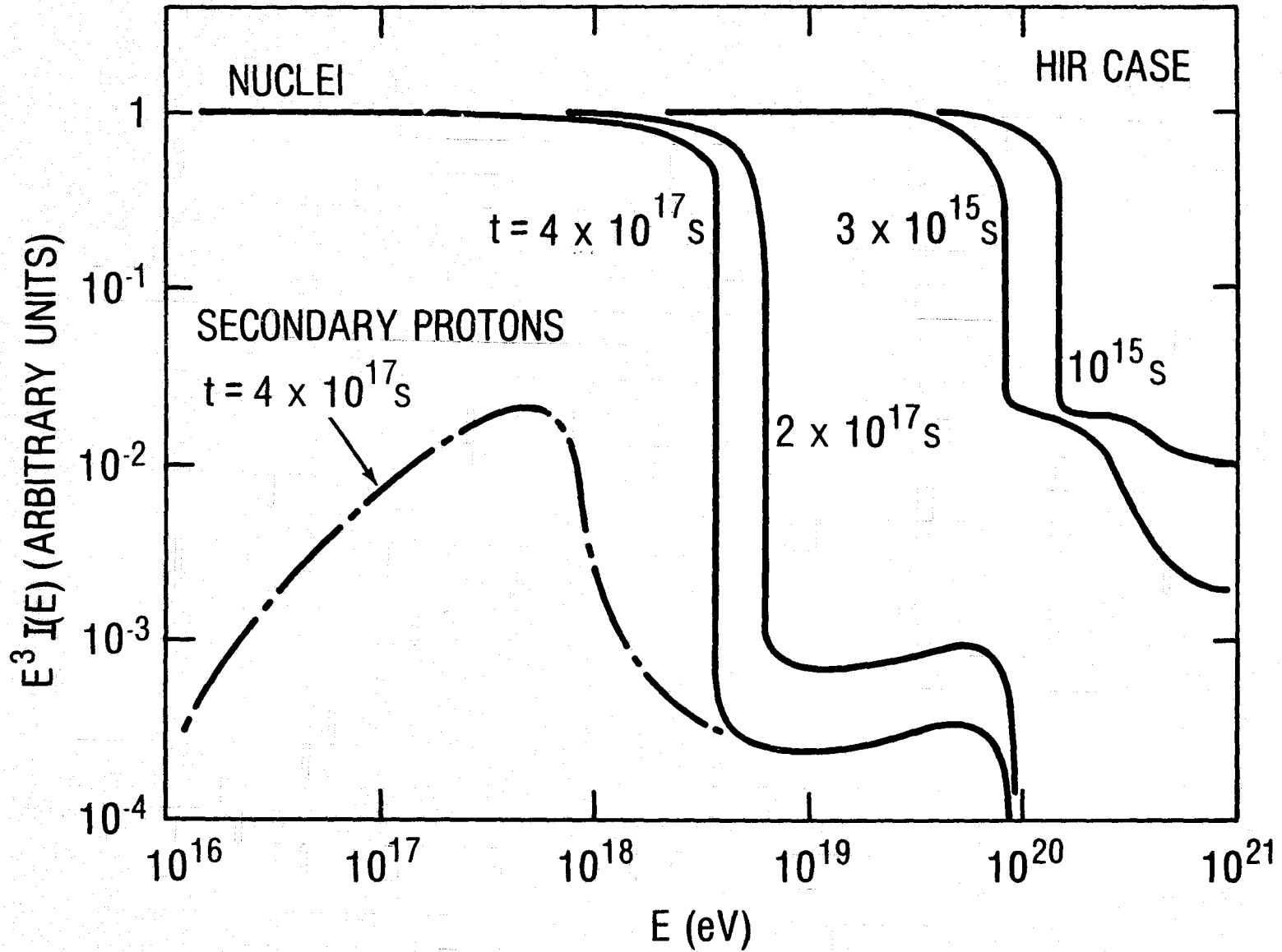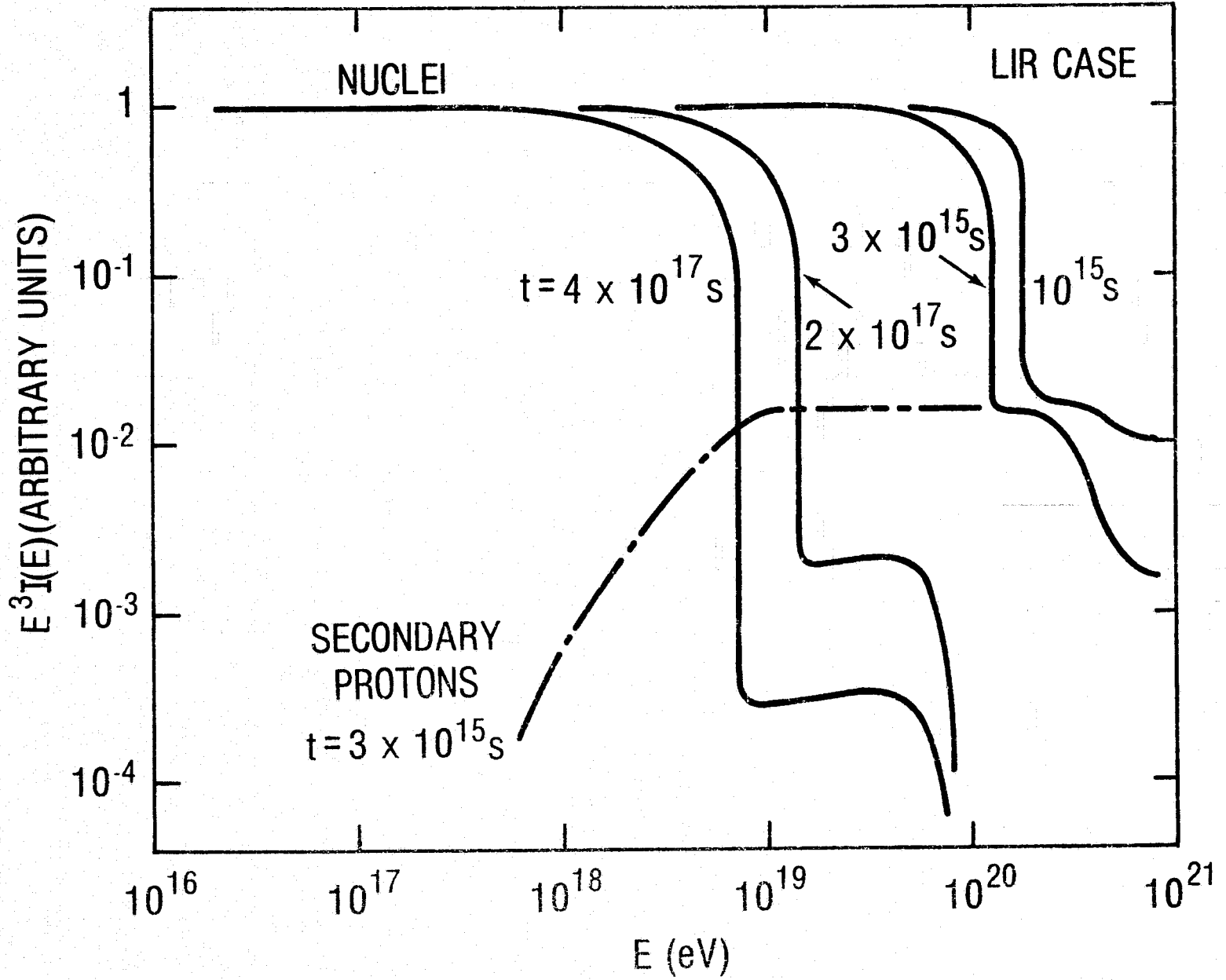
FIGURE 15

FIGURE 16

10^{21}

10^{20}

E_c, (eV)

10^{19}

10^{18}

10^{15} 10^{16} 10^{17} 10^{18}

t (s)